Dissolved organic matter from tropical peatlands reduces shelf sea light availability in the Singapore Strait, Southeast Asia

Author(s):
Martin, Patrick; Sanwlani, Nivedita; Lee, Tiffany Wan Qi; Wong, Joel Meng Cheng; Chang, Kristy Yi Wen; Wong, Elizabeth Wing-See; Liew, Soo Chin

Publication date:
2021-08-19

Permanent link:
https://doi.org/10.3929/ethz-b-000504639

Originally published in:
Marine Ecology Progress Series 672, https://doi.org/10.3354/meps13776

Vol. 672: 89–109, 2021
https://doi.org/10.3354/meps13776

MARINE ECOLOGY PROGRESS SERIES
Mar Ecol Prog Ser

Published August 19

Dissolved organic matter from tropical peatlands reduces shelf sea light availability in the Singapore Strait, Southeast Asia

Patrick Martin[1,*], Nivedita Sanwlani[1,5], Tiffany Wan Qi Lee[1], Joel Meng Cheng Wong[2,3], Kristy Yi Wen Chang[1,4], Elizabeth Wing-See Wong[2], Soo Chin Liew[2]

[1]Asian School of the Environment, Nanyang Technological University, 639798 Singapore
[2]Centre for Remote Imaging, Sensing, and Processing, National University of Singapore, 119076 Singapore

[3]*Present address:* Department of Environmental Systems Science, ETH Zürich, 8092 Zürich, Switzerland
[4]*Present address:* Singapore Centre for Environmental Life Sciences Engineering, Nanyang Technological University, 637551 Singapore
[5]*Present address:* Satellite Research Centre, School of Electrical and Electronic Engineering, Nanyang Technological University, 637553 Singapore

ABSTRACT: Shelf seas provide valuable ecosystem services, but their productivity and ecological functioning depend critically on sunlight transmitted through the water column. Anthropogenic reductions in underwater light availability are thus a serious threat to coastal habitats. The flux of light-absorbing coloured dissolved organic matter (CDOM) from land to sea may have increased world-wide, but how this has altered the availability and spectral quality of light in shelf seas remains poorly known. We present time-series data from the Sunda Shelf in Southeast Asia, where the monsoon-driven reversal in ocean currents supplies water enriched in CDOM from tropical peatlands for part of the year, resulting in 5- to 10-fold seasonal variation in light absorption by CDOM. We show that this terrigenous CDOM can dominate underwater light absorption at wavelengths up to 500 nm, and shift the underwater irradiance spectrum towards longer wavelengths. The seasonal presence of terrigenous CDOM also reduces the 10% light penetration depth by 1–5 m, or 10–45%. We estimate that on average 0.6 m, or 25%, of this terrigenous CDOM-mediated shoaling might be attributable to the enhanced input of dissolved organic matter following peatland disturbance. The seasonal change in the light environment is correlated with changes in phytoplankton absorption spectra that suggest a photo-acclimation response, and we infer that terrigenous CDOM likely contributes to limiting the depth distribution of photosynthetic corals. The results reveal an ecologically important but largely overlooked impact of human modifications to carbon fluxes that is likely increasingly important in coastal seas.

KEY WORDS: Coral reefs · Optical water quality · Underwater light attenuation · Coloured dissolved organic matter · Dissolved organic carbon · Tropical peatlands

1. INTRODUCTION

Shelf seas account for less than 10% of the global ocean area, but contribute more than 50% of the value of all marine ecosystem services (Costanza et al. 2014). These ecosystem services are largely contributed by benthic habitats that require sunlight for photosynthesis, such as coral reefs and seagrass beds. The attenuation of sunlight with depth is consequently a critical aspect of shelf sea water quality (Kirk 1988), and can significantly impact the productivity and areal extent of light-dependent benthic ecosystems (Gattuso et al. 2006). Changes in light attenuation and water clarity are therefore highly significant stressors of shelf-sea ecosystems (Dupont & Aksnes 2013, Filbee-Dexter & Wernberg 2018, Heery et al. 2018).

*Corresponding author: pmartin@ntu.edu.sg

Publisher: Inter-Research · www.int-res.com

Underwater light attenuation varies chiefly as a result of absorption and backscattering of light by phytoplankton, suspended organic detritus particles, suspended inorganic sediment particles, and dissolved organic matter (DOM). Each of these optically active constituents can contribute significantly to light attenuation in aquatic ecosystems (IOCCG 2000). Moreover, because their absorption and backscattering spectra differ, the attenuation of an equal amount of sunlight by different constituents results in a different spectral distribution of light underwater. DOM absorbs exponentially at short wavelengths in the ultraviolet (UV) and blue band, and therefore plays an important role in protecting marine organisms from photo-damage (Arrigo & Brown 1996, Banaszak & Lesser 2009, Häder et al. 2015). Yet by also absorbing blue light, DOM can shift the underwater irradiance to longer wavelengths that are less effectively absorbed by many photosynthetic organisms. Such spectral variation in the available light underwater can, for example, alter the phytoplankton community structure (Stomp et al. 2007, Gerea et al. 2017).

However, especially in the context of anthropogenic impacts on underwater light availability, the most widely recognised drivers of light attenuation in coastal waters are eutrophication (Dennison et al. 1993, Duarte 1995, Burkholder et al. 2007) and suspended sediment particles (Fabricius 2005, Storlazzi et al. 2015, Heery et al. 2018). In contrast, even though DOM can significantly alter the optical properties of coastal waters (DeGrandpre et al. 1996, Kowalczuk et al. 2005, Foden et al. 2008, Kuwahara et al. 2010, Mascarenhas et al. 2017, Petus et al. 2018), the potential for DOM to drive ecologically significant changes in light attenuation, and the consequences for the spectral quality of underwater irradiance, are often neglected outside of the optical oceanography literature.

The light absorbing substances in the DOM pool, such as humic substances, are collectively known as coloured dissolved organic matter (CDOM). Although CDOM is also produced by bacteria and phytoplankton in the ocean (Coble 2007, Dainard & Guéguen 2013, Osburn et al. 2019), DOM that originates from the partial decomposition of terrestrial vegetation is particularly light-absorbent (Vantrepotte et al. 2015, Massicotte et al. 2017). The flux of this CDOM-rich terrigenous dissolved organic carbon (terrigenous DOC, or tDOC) from land to coastal oceans is a quantitatively significant part of the global carbon cycle and has increased significantly in many parts of the world (Evans et al. 2005, Monteith et al. 2007, Moore et al. 2013). In Europe and North America, these trends may be largely driven by the recent reductions in atmospheric acid deposition, because acid deposition reduces soil organic matter solubility (Skjelkvåle et al. 2005, Evans et al. 2006, Monteith et al. 2007). However, climate warming, increased water run-off, and land-use change are also driving increased tDOC fluxes in both high- and low-latitude regions (Hessen et al. 2010, Larsen et al. 2011, Weyhenmeyer et al. 2012, Moore et al. 2013, de Wit et al. 2016, Noacco et al. 2017, Wauthy et al. 2018). CDOM is an integral part of tDOC, and the concentrations of tDOC and of CDOM are therefore highly correlated in rivers and river plumes (Fichot & Benner 2011, Massicotte et al. 2017, Martin et al. 2018). Thus, increases in tDOC flux to coastal waters will necessarily entail increases in terrigenous CDOM flux. Moreover, tDOC and associated CDOM frequently mix conservatively across salinity gradients in estuaries and shelf seas (Fichot & Benner 2012, Chen et al. 2015, Martin et al. 2018, Painter et al. 2018), such that shelf seas and adjacent oceanic regions can have high concentrations of tDOC and terrigenous CDOM (Blough et al. 1993, Kaiser et al. 2017, Medeiros et al. 2017, Carr et al. 2019, Zhou et al. 2019). Terrigenous CDOM thus has the potential to be advected far across shelf seas, and increases in tDOC flux might therefore affect the light environment over large areas of coastal ocean.

The fact that terrigenous, as opposed to marine, CDOM can significantly affect the underwater light environment in the sea has been recognised in regions where the CDOM pool is predominantly terrestrial in origin (Blough et al. 1993, Kjeldstad et al. 2003, Kowalczuk et al. 2006, Hessen et al. 2010, Mizubayashi et al. 2013, Cherukuru et al. 2014). However, CDOM in coastal waters often consists of a mixture of marine and terrigenous CDOM in proportions that can vary spatially and temporally. The most common way to distinguish marine from terrigenous CDOM is by measuring the slope of the CDOM absorption spectrum, originally over large wavelength ranges from UV to visible bands (Stedmon & Markager 2001, Kowalczuk et al. 2006, Astoreca et al. 2009). More recently, spectral slopes over narrow ranges of shorter wavelengths have become increasingly established for identifying terrigenous CDOM in terrestrially influenced waters, especially the spectral slope (S) between 275 and 295 nm, $S_{275–295}$ (Helms et al. 2008, Vantrepotte et al. 2015, Lu et al. 2016, Medeiros et al. 2017, Carr et al. 2019, Signorini et al. 2019). $S_{275–295}$ has also been used successfully to quantify tDOC concentrations in shelf seas (Fichot & Benner 2012, Fichot et al. 2013, 2014).

However, although the importance of terrigenous CDOM for the light environment of coastal waters has clearly been recognised, the relative contributions of terrigenous and marine CDOM to light attenuation in shelf seas have not been partitioned quantitatively. Consequently, although large-scale anthropogenic changes in land–ocean tDOC fluxes have the potential to alter the light environment of shelf seas by altering the terrigenous CDOM concentration, our knowledge of such impacts is still limited. Based on long-term trends in salinity and correlations between salinity and CDOM in Norwegian fjords, Aksnes et al. (2009) inferred that increased terrigenous CDOM had resulted in 'coastal browning', possibly contributing to mesopelagic regime shifts from fish (visual predators) to jellyfish (tactile predators). Similarly, an increase in non-autotrophic particulate organic carbon in southern Norway was interpreted as indicating an increase in terrigenous CDOM, and this was hypothesised to have contributed to the collapse of kelp forests (Frigstad et al. 2013). An increase in terrigenous CDOM was also implicated as a driver of decreased water clarity in the North Sea (Dupont & Aksnes 2013), which may have delayed the spring phytoplankton bloom by up to 3 wk (Opdal et al. 2019). Ecosystem modelling has additionally shown that increased terrigenous CDOM absorption can lead to a shallower distribution of phytoplankton and a shallower nutricline, resembling symptoms of eutrophication (Urtizberea et al. 2013). Moreover, time series of recent CDOM and historical chromaticity data suggest that terrigenous CDOM concentrations in the Gulf of Maine have increased as a result of greater river run-off (Balch et al. 2012, 2016). Yet overall, it remains unclear to what extent coastal browning due to terrigenous CDOM has impacted shelf sea ecosystems and productivity.

This contrasts with our better understanding of the ecological impacts of freshwater 'lake browning' caused by rising inputs of tDOC and terrigenous CDOM (Larsen et al. 2011, Graneli 2012, Wauthy et al. 2018). These impacts include reductions in primary productivity, shifts from benthic to pelagic primary productivity, thermocline shoaling, and possibly reductions in stocks of visually hunting fish (Ask et al. 2009, Thrane et al. 2014, Solomon et al. 2015). However, the freshwater lakes where lake browning has been reported contain far higher concentrations of terrigenous CDOM than do shelf seas, so much so that filtered lake water can have a noticeably yellow-brown colouration (Solomon et al. 2015). Whether CDOM-mediated browning can affect the ecological functioning of shelf seas to the same degree as lakes is still unclear.

Here, we used biogeochemical and optical time-series data from the Singapore Strait in the Sunda Shelf Sea in Southeast Asia to estimate seasonal changes in the proportion of marine and terrigenous CDOM, and to quantify how terrigenous CDOM impacts underwater light availability. Tropical peatlands are the dominant source of tDOC and terrigenous CDOM in this part of Southeast Asia (Baum et al. 2007, Siegel et al. 2019). Previous research suggests that the extensive and recent anthropogenic disturbance and drainage of these peatlands (Miettinen et al. 2016) have increased peatland tDOC flux by about 50% (Moore et al. 2013, Yupi et al. 2016). Given that tDOC and CDOM show a strong relationship in Southeast Asian peatlands (Cook et al. 2017, Martin et al. 2018), we present a first-order estimate of the potential anthropogenic contribution to CDOM-mediated light attenuation.

2. MATERIALS AND METHODS

2.1. Study area

The Singapore Strait is located in the central Sunda Shelf Sea in Southeast Asia, close to the peatlands on Sumatra (Fig. 1). Ocean currents on the Sunda Shelf reverse direction seasonally (van Maren & Gerritsen 2012, Mayer & Pohlmann 2014, Susanto et al. 2016): during the Northeast (NE) Monsoon (November–February), water flows westwards from the South China Sea through the Singapore Strait, and further northwards through the Malacca Strait to the Indian Ocean. During the Southwest (SW) Monsoon (May–September), the flow through the Malacca Strait stagnates or reverses direction, and water flows eastwards from the coast of Sumatra back through the Singapore Strait (Fig. 1). The annual mean flow is westwards from the South China Sea through the Singapore Strait and northward through the Malacca Strait to the Indian Ocean, with water residence times of 1–2 yr over most of the shelf (Mayer et al. 2015, 2018). The central Sunda Shelf (southern Malacca Strait, Singapore Strait, and Karimata Strait) also experiences strong tidal currents that mix the water column all the way to the seafloor and prevent stratification (Mayer & Pohlmann 2014, Hamzah et al. 2020). Thus, water from the open South China Sea reaches Sumatra, receives large inputs of CDOM-rich tDOC from the peatlands, and then seasonally flows back into the Singapore Strait, while over the

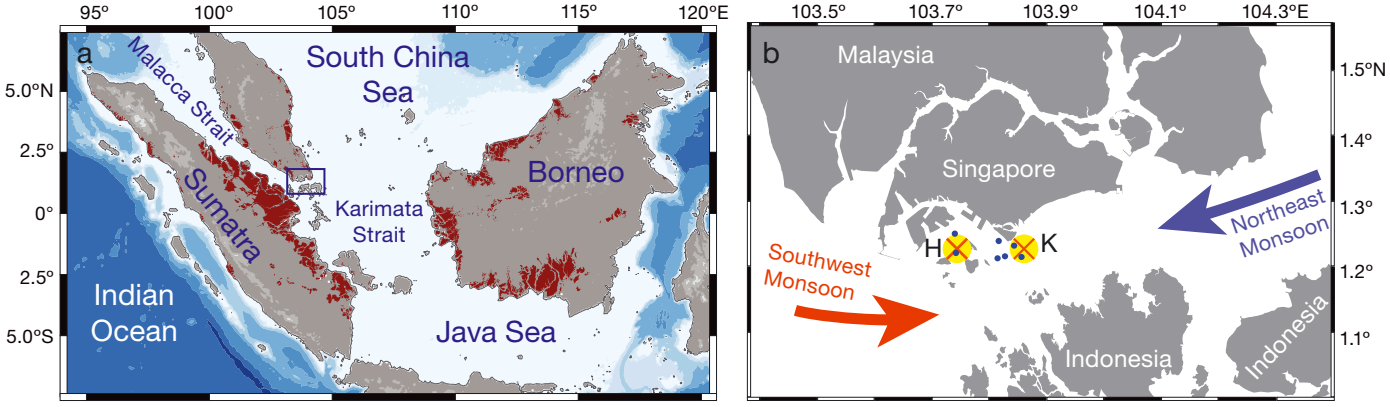

Fig. 1. (a) Study region showing location of peatlands (dark red shading) and ocean bathymetry; the blue box corresponds to the area shown in (b). (b) Singapore Strait, with the red and blue arrows showing the mean current direction during each monsoon season. The 2 main sampling sites are marked by the yellow circles with red crosses: the eastern site, Kusu (K), is exposed, while the western site, Hantu (H), is sheltered. Other stations that were sampled occasionally are shown as small blue dots

longer term, it flows towards the Indian Ocean via the Malacca Strait and the Java Sea. For the present analysis, we defined the seasons as follows: Inter-monsoon 1: 1 March to 14 May; SW Monsoon: 15 May to 14 September; Inter-monsoon 2: 15 September to 14 November; NE Monsoon: 15 November to end of February.

2.2. Field sampling and sensor measurements

The present analysis uses data collected as part of an ongoing biogeochemical time-series programme. Salinity, DOC, and CDOM were measured at monthly to biweekly frequency between October 2017 and August 2020. Bio-optical parameters (particulate absorption and backscattering) were measured approximately monthly between December 2018 and August 2020. We collected samples at 2 sites (Fig. 1): Kusu Island (an exposed site experiencing higher wave energy) and Hantu Island (a sheltered site with lower wave energy). Both islands have artificial breakwaters, and narrow coral reefs that extend about 20 m horizontally from the breakwaters. Additional sites between Kusu and Hantu were sampled occasionally to constrain spatial variability (Fig. 1). Conductivity-temperature-depth profiles were measured with a Valeport FastCTD at 16 Hz to 12–15 m depending on current and bottom depth; stratification was not observed. Water was collected adjacent to the reefs at 5 m depth using a Niskin bottle. Samples for CDOM and DOC analysis were filtered on board through 0.2 µm Supor polyethersulfone filters (all tubing and filter housings were cleaned with 1 M HCl, then assembled with the filters and pre-rinsed with 200 ml of ultrapure water [18.2 MΩ cm^{-1}] and with sample water) and stored in 40 ml amber borosilicate vials (pre-baked at 450°C for 4 h) with Teflon-coated septa. Water for chlorophyll *a* (chl *a*) and particulate absorption was stored in acid-washed high density polyethylene bottles in the dark and filtered (25 mm Whatman GF/F) 3–6 h later in the laboratory.

Backscattering was measured at 412, 440, 488, 510, 532, 595, 650, 676, and 715 nm using a Wetlabs BB9 lowered to 1 m depth; 60 consecutive measurements were taken at 1 Hz and averaged. The data were processed according to the manufacturer's instructions: the raw measurement was converted to the total volume scattering coefficient by subtracting the dark offset (measured before each field trip) and multiplying by a calibration scaling factor, and corrected for non-water absorption as measured by a TriOS OSCAR instrument. Volume scattering from pure seawater was subtracted and the particulate scattering converted to particulate backscattering coefficients following Boss & Pegau (2001), which were then fit with a power law at 1 nm resolution over the wavelength range of photosynthetically active radiation (PAR, 400–700 nm).

The present analysis focusses on December 2018 to August 2020, during which we acquired 77 measurements of CDOM, DOC, and salinity, 60 measurements of particulate absorption, and 36 measurements of backscattering. The CDOM and salinity time-series data are also presented in a separate analysis focussing on carbon biogeochemistry by Zhou et al. (2021).

2.3. CDOM and particulate absorption measurements

CDOM samples were stored at +4°C back on land and analysed within 24 h of collection. Samples were brought to room temperature and absorbance was measured from 250 to 800 nm at 1 nm resolution in 10 cm pathlength quartz cuvettes on a Thermo Evolution300 dual-beam spectrophotometer against ultrapure water as a reference. Data were baseline-corrected according to Green & Blough (1994), smoothed using a loess function, and converted to Napierian absorption coefficients, using the R package 'hyperSpec' (Beleites & Sergo 2018). Here, we express the concentration of CDOM as the CDOM absorption coefficient at 440 nm, $a_{CDOM}(440)$, with units of m^{-1}. We also calculated the CDOM spectral slope from 275 to 295 nm, $S_{275\text{-}295}$, and the spectral slope ratio (S_R, the ratio of the 275–295 nm slope to the 350–400 nm slope) following Helms et al. (2008). Both $S_{275–295}$ and S_R have been shown to correlate with DOM apparent molecular weight (Helms et al. 2008) and are widely used as markers of tDOC in coastal seas (Fichot & Benner 2012, Fichot et al. 2013, Vantrepotte et al. 2015, Lu et al. 2016, Medeiros et al. 2017, Painter et al. 2018, Carr et al. 2019). To test whether seasonal variation in CDOM could be explained by conservative mixing between terrigenous CDOM (with low $S_{275–295}$ and S_R) and marine CDOM (with high $S_{275–295}$ and S_R), we calculated a theoretical mixing model between the CDOM spectra measured on 15 March 2019 (with high $S_{275–295}$ and low $a_{CDOM}(440)$) and 16 July 2020 (lowest $S_{275–295}$ and highest $a_{CDOM}(440)$ in 2019 and 2020) as follows:

$$a_{CDOM,mix}(\lambda) = a_{CDOM,terr}(\lambda) \times f_{terr} + a_{CDOM,mar}(\lambda) \times (1 - f_{terr}) \quad (1)$$

where $a_{CDOM,mix}(\lambda)$ is the predicted CDOM spectrum for conservative mixing, $a_{CDOM,terr}$ and $a_{CDOM,mar}$ are the measured CDOM spectra at Hantu Island on 16 July 2020 and 15 March 2019, respectively, and f_{terr} is the fractional contribution of the 16 July 2020 spectrum (which we varied between 0 and 1 in increments of 0.0125 to simulate conservative mixing). For each predicted $a_{CDOM,mix}$ spectrum, $S_{275–295}$ and S_R were recalculated as for the original data. The theoretical mixing curves were plotted together with the measured data on scatter plots of $S_{275–295}$ and S_R against $a_{CDOM}(440)$, following Stedmon & Markager (2001).

Samples for particulate absorption (500–1000 ml) were vacuum-filtered onto 25 mm diameter Whatman GF/F filters and stored in liquid nitrogen in embedding cassettes (Kartell Labware) wrapped in aluminium foil. Samples were thawed to room temperature, moistened briefly on a sponge soaked in filtered seawater, and absorbance was measured from 300 to 800 nm with filters held inside an integrating sphere using a centre-mount sample holder on a PerkinElmer Lambda 950 spectrophotometer, as recommended by Stramski et al. (2015). Multiple blank filters were measured throughout each batch analysis. Filters were then depigmented (as assessed by the complete disappearance of the chl *a* absorption peak at 668 nm) with 5 ml of 0.1% sodium hypochlorite in ultrapure water with 60 g l^{-1} sodium sulphate for 15 min (Ferrari & Tassan 1999), rinsed with 5 ml ultrapure water, and remeasured. All blank and sample absorbance spectra were first corrected for baseline drift by subtracting the mean absorbance from 801 to 851 nm from the rest of the spectrum, and then blank-corrected by subtracting the mean baseline drift-corrected blank spectrum from all sample absorbance spectra. These corrected sample absorbances were then corrected for pathlength amplification according to Stramski et al. (2015):

$$A_s = 0.323(A_f)^{1.0867} \quad (2)$$

where A_s is the pathlength-corrected sample absorbance, and A_f is the blank- and baseline-corrected absorbance of each filter. Corrected absorbances were then converted to Napierian absorption coefficients by accounting for the area of sample on each filter (the filtered area of each filter had a radius of 11.5 mm) and the sample volume filtered. Phytoplankton absorption (a_{phyto}) was calculated by subtracting the depigmented absorption spectrum (i.e. the non-algal particulate absorption, a_{NAP}) from the total particulate absorption spectrum. From the a_{phyto} spectra, we further calculated the phytoplankton absorption spectral slope following Eisner et al. (2003):

$$a_{phyto}\ \text{slope} = \frac{a_{phyto}(488) - a_{phyto}(532)}{a_{phyto}(676) \times (488 - 532)} \quad (3)$$

where numbers in parentheses indicate the wavelengths. We also calculated the ratio of phytoplankton absorption at 490 to 510 nm, $a_{phyto}(490)$: $a_{phyto}(510)$, following Hickman et al. (2009). Both of these are measures of the ratio of photoprotective to photosynthetic carotenoid pigments in the phytoplankton community, which is indicative of photoacclimation.

Seasonal average spectral absorption budgets were calculated as the fractional contribution of each absorbing constituent (CDOM, non-algal particles,

phytoplankton, and water) to the total absorption at each wavelength, and then averaging these data seasonally.

2.4. DOC analysis and specific UV absorbance calculation

DOC samples (30 ml) were acidified with 100 µl of 50% H_2SO_4 in the field, stored at +4°C, and analysed within 2–3 mo of collection on a Shimadzu TOC-L analyser with the Shimadzu high-salt combustion kit and calibrated using potassium hydrogen phthalate, as in previous work (Martin et al. 2018). Certified reference material from the University of Miami, USA (deep-sea water, 42–45 µmol l^{-1} DOC), was analysed alongside every batch of measurements, and returned a long-term mean ± SD of 48.0 ± 3.9 µmol l^{-1} throughout our time series. DOC samples were collected and analysed in triplicate starting in December 2018. We used these data to calculate the specific UV absorbance at 254 nm ($SUVA_{254}$):

$$SUVA_{254} = \frac{A_{254}}{[DOC]} \quad (4)$$

where A_{254} is the CDOM absorbance at 254 nm m^{-1}, and the DOC concentration is in mg C l^{-1} (note that the absorbance is obtained by dividing the Napierian absorption coefficient by 2.303). $SUVA_{254}$ consequently has units of l mg^{-1} m^{-1}, and is a measure of DOM aromaticity (Traina et al. 1990, Weishaar et al. 2003). Similar to $S_{275–295}$ and S_R, $SUVA_{254}$ is useful as a tracer of terrigenous DOM in aquatic ecosystems (Anderson et al. 2019, Carr et al. 2019).

2.5. Chl *a*

Samples for chl *a* (200–1000 ml) were filtered onto 25 mm diameter Whatman GF/F filters, wrapped in aluminium foil, flash-frozen in liquid nitrogen, and stored at −80°C until analysis within 3 mo. Filters were then extracted in 90% acetone at 4°C in the dark overnight, briefly centrifuged to remove particles, and fluorescence was measured on a Horiba Fluoromax4 at excitation 436 nm and emission 680 nm with slit widths of 5 nm (Welschmeyer 1994). Fluorescence was acquired as the fluorescence signal normalised to the lamp reference measurement to account for variation in lamp intensity (using the Fluoromax4 S1c/R1c acquisition mode), and calibration was performed with a spinach chl *a* standard (Sigma-Aldrich, C5753-1MG).

2.6. Calculating light-attenuation spectra

Underwater light attenuation can be described by the diffuse attenuation coefficient of downwelling irradiance, K_d, which varies spectrally:

$$E_d(z,\lambda) = E_d(0,\lambda) \times e^{K_d(\lambda)\times z} \quad (5)$$

where $E_d(z,\lambda)$ is the downwelling irradiance at depth z and wavelength λ, $E_d(0,\lambda)$ is the downwelling irradiance at wavelength λ at the surface, and $K_d(\lambda)$ is the diffuse attenuation coefficient at wavelength λ. We used our spectral measurements of absorption by CDOM and particles, and backscattering by particles, to calculate spectra of K_d over the wavelength range 400–700 nm according to Lee et al. (2005):

$$K_d \,(1 + 0.005\theta)a + 4.18(1 - 0.52e^{-10.8a})b_b \quad (6)$$

where θ is the solar zenith angle, a is total absorption, and b_b is total backscattering. Absorption and backscattering spectra of pure seawater were taken from Pope & Fry (1997) and Smith & Baker (1981), respectively. We used θ at solar noon on each date (i.e. the time of day when the sun is at its highest point), such that the result reflects the maximum light penetration for each date. θ and solar noon times were calculated using the R packages 'GeoLight' (Lisovski & Hahn 2012) and 'suncalc'. This calculation was originally developed to estimate K_d between the surface and the depth to which 10% of surface PAR penetrates ($Z_{10\%}$) and was therefore denoted $K_d(E_{10\%})$ by Lee et al. (2005); we refer to this as K_d for simplicity, since K_d at individual wavelengths does not vary strongly with depth unless the absorption and backscattering spectra vary with depth. A total of 32 concomitant measurements of absorption and backscattering were available for this calculation, taken on 17 separate dates. We verified that this calculation yielded accurate estimates of K_d by comparing calculated K_d spectra to K_d spectra measured using a TriOS RAMSES radiometer at 19 of the 32 stations; the radiometer measurement methods and the results of this comparison are shown in Text S1 and Figs. S1 & S2 in the Supplement at www.int-res.com/articles/suppl/m672p089_supp.pdf.

2.7. Calculating underwater irradiance spectra and depth of PAR penetration

To examine how seasonal variation in absorption and backscattering affect both the spectral quality of irradiance underwater and the depth to which PAR penetrates, we used the K_d spectra together with

modelled mid-day solar irradiance for each date to calculate depth profiles of underwater irradiance, the vertical attenuation coefficient of downwelling PAR, K_d(PAR), and $Z_{10\%}$. The downwelling irradiance spectrum just below the water surface (E_d0^-) was generated using the Hydrolight model for solar noon on each date, assuming 20% cloud cover and 2 m s^{-1} wind speed. Our purpose with these calculations was not to estimate actual daily light doses underwater, which depend especially on cloud cover, but to examine how the depth penetration and spectral distribution of underwater light vary over time. Since cloud cover chiefly alters the total irradiance rather than the shape of the irradiance spectrum, it has little impact on underwater irradiance spectral shape and depth penetration; modelled surface irradiance is hence sufficient for this purpose.

We first calculated the average underwater irradiance spectrum experienced by phytoplankton in a fully mixed water column, $E_d(Z_{mean})$ (Ferrero et al. 2006, Gerea et al. 2017):

$$E_d(Z_{mean}) = E_d0^- \frac{1-e^{-K_dZ}}{K_dZ} \quad (7)$$

where Z is the depth of the water column. We selected 30 m, which is representative of much of the Singapore Strait surrounding our sampling sites (Chan et al. 2006).

Next, to examine how the spectral light quality experienced by benthic organisms is affected, we calculated the underwater irradiance spectrum at fixed depths within the upper 10 m for each date by attenuating the Hydrolight-modelled noon-time E_d0^- spectra with the calculated K_d spectra according to Eq. (5).

Finally, to examine how the overall depth of light penetration varied, we calculated K_d(PAR) and $Z_{10\%}$. To do this, we first attenuated the modelled E_d0^- spectra with the calculated K_d spectra (Eq. 5) at 0.1 m intervals down to a depth of 20 m to yield calculated depth profiles of downwelling irradiance. The downwelling irradiance spectra were converted to a total photon flux of PAR from 400 to 700 nm as described in Text S1. K_d(PAR) was then calculated as the slope of a linear regression of the natural log of PAR flux versus depth, and $Z_{10\%}$ was calculated as 2.303/K_d(PAR). Note that unlike K_d at individual wavelengths, K_d(PAR) changes significantly with depth because of the large spectral variation in $K_d(\lambda)$ (Lee 2009, Lee et al. 2018). Consequently, the value of K_d(PAR) calculated by regressing PAR against depth varies depending on the depth to which the regression is performed. We used an empirical relationship from our measured radiometer data (Fig. S3) to determine the appropriate depth interval over which to perform the regression, as described in Text S1.

2.8. Impact of terrigenous CDOM on $Z_{10\%}$

Our time-series of $S_{275–295}$, S_R, and $SUVA_{254}$ indicated that the variation in CDOM absorption is predominantly the result of conservative mixing between terrigenous CDOM and marine CDOM, as shown in Section 3.1. Based on these data, the CDOM during the March–April inter-monsoon period was predominantly marine, while the CDOM during other periods consisted of a mixture of this background level of marine CDOM and a varying amount of terrigenous CDOM. We therefore quantified the amount of terrigenous CDOM in each sample by subtracting the inter-monsoon CDOM spectrum measured on 15 March 2019 (which we also used as 1 endmember in our conservative mixing model; see Section 2.3) from the measured CDOM spectrum in each sample.

To quantify the impact of this terrigenous CDOM on the depth of PAR penetration, we recalculated our K_d spectra (Eq. 6) using the 15 March 2019 CDOM spectrum in place of the CDOM spectrum measured for each station. We then recalculated K_d(PAR) and $Z_{10\%}$, as well as $E_d(Z_{mean})$, as described in Section 2.7. This yielded estimates of what K_d(PAR), $Z_{10\%}$, and $E_d(Z_{mean})$ would have been at each station in the absence of terrigenous CDOM.

To quantify the potential anthropogenic contribution to CDOM-mediated light attenuation, we recalculated K_d again, this time with the terrigenous CDOM absorption reduced by 35% of the observed value. This is based on estimates from Borneo and Sumatra that land-use change has increased the flux of DOC from Southeast Asian peatlands by 54% (Moore et al. 2013, Yupi et al. 2016), and the fact that nearly all peatlands in the region have experienced disturbance (Miettinen et al. 2016). Because DOC and CDOM are very closely correlated in peatland-draining blackwater rivers and downstream coastal waters in Southeast Asia (Cook et al. 2017, Martin et al. 2018), these estimates imply that 35% of the observed terrigenous CDOM in peatland-influenced coastal waters is anthropogenic (if the modern, post-disturbance DOC flux is 1.54-fold greater than the pre-disturbance DOC flux, then the anthropogenic fraction of the modern DOC flux is 0.54/1.54 = 0.35). We only estimated this anthropogenic contribution for the SW Monsoon period, as this is the season when the Singapore

Strait receives terrestrial inputs from the large peatland areas on Sumatra.

3. RESULTS

3.1. Bio-optical time-series data

The concentration of CDOM, $a_{CDOM}(440)$, ranged from lowest values of 0.039–0.045 m^{-1} during both inter-monsoons to peak values of 0.27–0.45 m^{-1} during the May–September SW Monsoon (Fig. 2a). Smaller increases were also seen during the November–February NE Monsoon, with peak $a_{CDOM}(440)$ of 0.10–0.17 m^{-1}. During the SW Monsoon, the $S_{275–295}$ decreased from around 0.030 to ≤0.018 (Fig. 2b), and the S_R decreased from around 2.0 to <1.25 (Fig. 2c), while the $SUVA_{254}$ increased from <1.0 to mostly between 2.0 and 3.0 (Fig. 2d). Smaller decreases in $S_{275–295}$ and S_R, and increases in $SUVA_{254}$, were also seen during the NE Monsoon. Salinity decreased from values of 32–33 during the inter-monsoons to 31–32 during the NE Monsoon and even lower to 29–31 during the SW Monsoon (Fig. 2e). Additional data collected in 2018 show that the seasonal increases in CDOM and $SUVA_{254}$, and decreases in salinity,

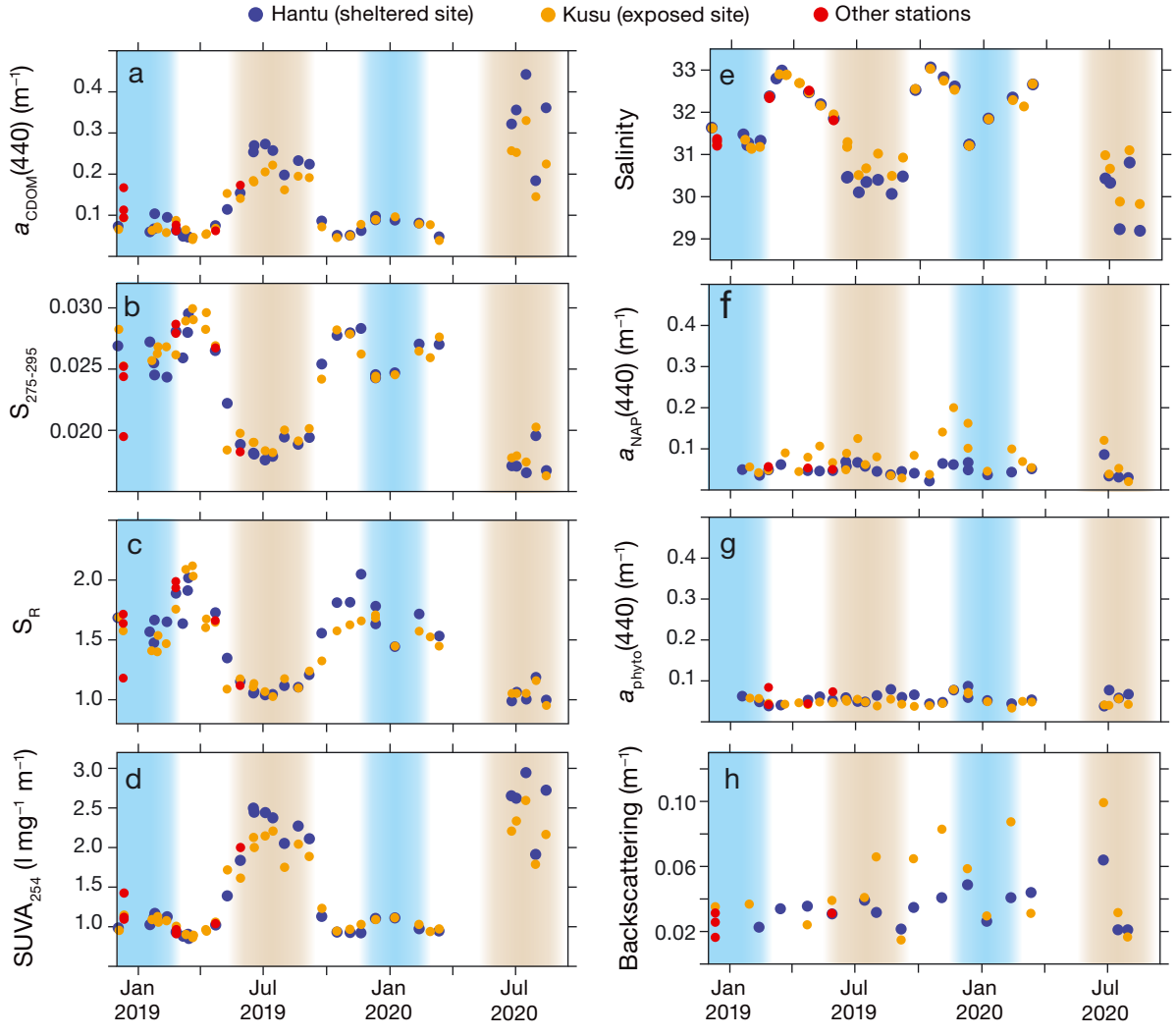

Fig. 2. Biogeochemical and optical time-series data. (a) Absorption coefficient of coloured dissolved organic matter (CDOM) at 440 nm ($a_{CDOM}(440)$), (b) CDOM spectral slope (S) between 275 and 295 nm ($S_{275–295}$), (c) CDOM spectral slope ratio (S_R), (d) specific UV absorbance at 254 nm ($SUVA_{254}$), and (e) seawater salinity all showed seasonal variation consistent with a large input of terrigenous CDOM during the Southwest Monsoon (brown shading), and to a lesser extent during the Northeast Monsoon (blue shading). In contrast, time series of absorption by (f) non-algal particles (a_{NAP}) and (g) phytoplankton a_{phyto}, (both at 440 nm), and (h) backscattering by particles (at 440 nm) showed no clear seasonality, but absorption by non-algal particles and particulate backscattering were quite variable and typically higher at the more exposed site

$S_{275\text{-}295}$, and S_R were similar to those in 2020, confirming that large and sustained inputs of CDOM are typical during the SW Monsoon (Fig. S4; particulate optical properties were not measured until 2019). The seasonal differences in $a_{CDOM}(440)$, $S_{275–295}$, S_R, $SUVA_{254}$, and salinity were significant (Kruskal-Wallis test, all $\chi^2 > 77$, df = 3, all $p < 0.001$).

Absorption by phytoplankton, non-algal particles, and particulate backscattering showed no significant differences between seasons (Kruskal-Wallis test, all $\chi^2 < 6.2$, df = 3, all $p > 0.10$), although the more exposed site (Kusu) typically had higher non-algal particulate absorption and particulate backscattering (Fig. 2f–h). Particulate backscattering at 440 nm was highly correlated with particulate backscattering at all other wavelengths (Fig. S5; all Pearson's correlation coefficients >0.97). Consistent with the low phytoplankton absorption, chl *a* concentrations were relatively low (mean ± SD of 1.0 ± 0.5 µg l^{-1}; Fig. S6) and not significantly different between seasons (Kruskal-Wallis test, $\chi^2 = 2.9$, df = 3, $p = 0.40$).

We found that $S_{275–295}$ and S_R showed tight, inverse relationships with $a_{CDOM}(440)$ across all seasons (Fig. 3a,b), which closely followed the theoretical mixing model (Eq. 1; grey curves in Fig. 3a,b) between the CDOM spectra measured on 15 March 2019 (Inter-monsoon 1) and on 16 July 2020 (SW Monsoon). Note that CDOM spectral slope parameters show non-linear changes during conservative mixing (Stedmon & Markager 2003). Moreover, there was a significant, positive correlation between $a_{CDOM}(440)$ and $SUVA_{254}$ (Fig. 3c; Spearman's rank correlation, $\rho = 0.906$, $p < 0.001$, n = 129).

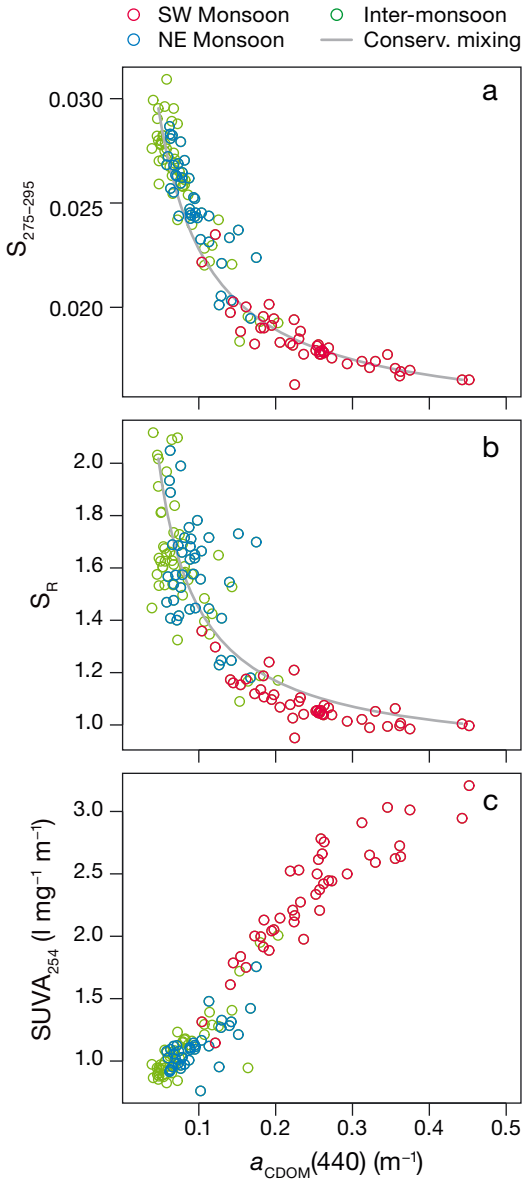

Fig. 3. Relationships between coloured dissolved organic matter (CDOM) absorption at 440 nm and (a) $S_{275–295}$, (b) S_R, and (c) $SUVA_{254}$ (definitions as in Fig. 2). Grey curves in (a,b) show predicted variation from the conservative mixing between the marine CDOM spectrum measured on 15 March 2019 and the primarily terrigenous CDOM spectrum measured on 16 July 2020. Data from the SW Monsoon consistently show high CDOM absorption associated with low $S_{275–295}$, low S_R, and high $SUVA_{254}$, indicative of a primarily terrigenous CDOM pool during this season

3.2. Seasonal changes in light absorption budgets, underwater irradiance, and phytoplankton absorption

The large seasonal changes in CDOM absorption altered the average spectral light absorption budget between seasons (Fig. 4). Absorption in the UV range (300–400 nm) was dominated by CDOM in all seasons, but to a greater extent in the SW Monsoon. Between 400 and 500 nm, CDOM dominated progressively less, and especially in the inter-monsoon seasons, the absorption by CDOM at 500 nm was only around 20% of the total absorption (Fig. 4a,c). In the SW Monsoon, however, CDOM contributed ≥50% of the total absorption up to 500 nm, and still contributed 50% of the non-water absorption up to 600 nm (Fig. 4b). During the NE Monsoon, the absorption budget was relatively less CDOM-dominated than in the SW Monsoon, but more than during both inter-monsoon seasons at similar wavelengths (Fig. 4e). In all seasons, absorption by non-algal particles was greater than phytoplankton absorption from 300 nm to roughly 440 nm, then up to 500–

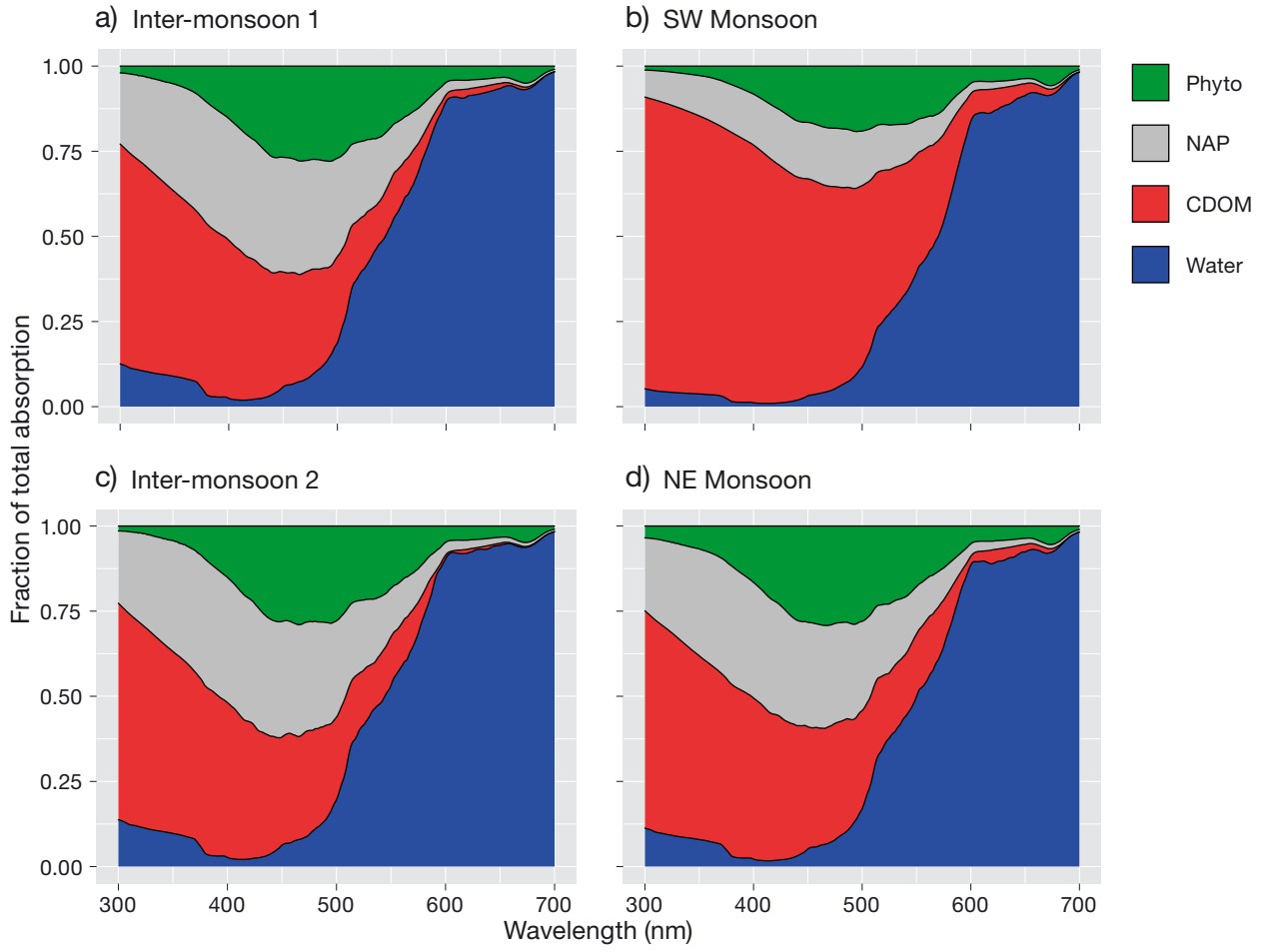

Fig. 4. Light absorption budgets across the ultraviolet and visible wavelengths. Data are seasonal means across all stations. Phyto: absorption by phytoplankton; NAP: absorption by non-algal particles; CDOM: absorption by coloured dissolved organic matter; Water: absorption by seawater

550 nm phytoplankton and non-algal particles contributed roughly equally, and phytoplankton increasingly dominated the particulate absorption from 550 to 700 nm. Water always contributed >50% of absorption from 550 to 700 nm (Fig. 4).

Using the modelled surface irradiance for solar noon on each sampling date, we found that the wavelength of peak irradiance shifted from 531 to 539 nm during both inter-monsoons and the NE Monsoon to between 547 and 566 nm in the SW Monsoon (Fig. 5). Similarly, the ratio of blue to green irradiance, $E_d(440)$ to $E_d(550)$, at each depth was significantly lower during the SW Monsoon than other seasons (Kruskal-Wallis test, all $\chi^2 \geq 13.5$, df = 3, all $p < 0.005$), indicating a seasonal decrease in the availability of blue light relative to longer wavelengths. This spectral shift in the underwater irradiance was also evident in the average irradiance experienced by phytoplankton under turbulent mixing (Eq. 7), which peaked at 567 nm during the SW Monsoon, but at 537–538 nm during the other seasons (Fig. 6). The ratio of blue to green irradiance was also significantly lower during the SW Monsoon (mean ratio of 0.46) compared to the other seasons (mean ratios of 0.54–0.62) for these averaged irradiances (Kruskal-Wallis test, $\chi^2 = 25.9$, df = 3, $p < 0.001$).

The phytoplankton absorption spectra revealed a statistically significant decrease in the ratio of $a_{phyto}(490)$ to $a_{phyto}(510)$ and a significant increase in the a_{phyto} spectral slope during the SW Monsoon (Fig. 7; Kruskal-Wallis test; both $\chi^2 \geq 12.4$, df = 3, both $p \leq 0.006$). Both the ratio of $a_{phyto}(490)$ to $a_{phyto}(510)$ and the a_{phyto} spectral slope were also significantly correlated with $a_{CDOM}(440)$ (Spearman's rank correlation; $\rho = -0.45$ and 0.39; both $p < 0.003$) and with $S_{275–295}$ (Spearman's rank correlation; $\rho = 0.50$ and −0.43; both $p < 0.001$).

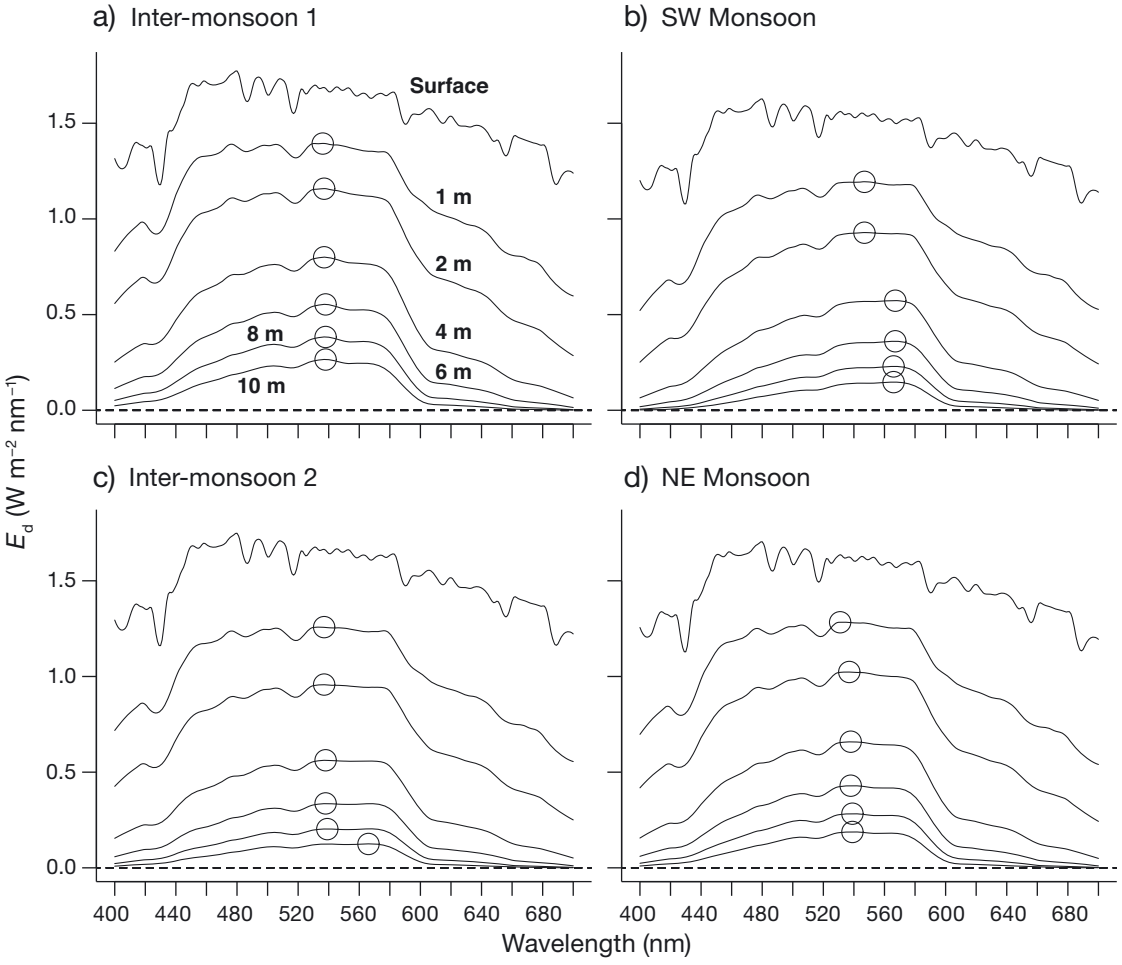

Fig. 5. Seasonal average downwelling irradiance (E_d) spectra calculated for solar noon at fixed depths for (a) March–May Inter-monsoon 1, (b) Southwest Monsoon, (c) September–November Inter-monsoon 2, and (d) Northeast Monsoon. Circles indicate the wavelength of maximum irradiance for each spectrum. The depths for spectra in panels (b–d) are as in panel (a)

3.3. $Z_{10\%}$ and impacts of terrigenous CDOM

$Z_{10\%}$ ranged between 3.7 and 9.8 m, with an overall average of 7.1 m, and was typically deeper at the more sheltered site (Fig. 8a). Across both sites, $Z_{10\%}$ was on average deepest during Inter-monsoon 1 (8.6 m) and shallowest during the SW Monsoon (6.6 m); this seasonal difference was significant (Kruskal-Wallis test, $\chi^2 = 8.4$, df = 3, p = 0.038), and corresponded to an average seasonal change in K_d(PAR) from 0.269 m^{-1} (Inter-monsoon 1) to 0.370 m^{-1} (SW Monsoon). To quantify the impact of terrigenous CDOM on the euphotic zone depth, we recalculated K_d(PAR) and $Z_{10\%}$ by using only the background marine CDOM spectrum measured on 15 March 2019 in place of the observed total CDOM absorption (see Section 2.8). We found that relative to the actually observed value of $Z_{10\%}$, the value of $Z_{10\%}$ without terrigenous CDOM was deeper by 0.7–4.9 m (on average, 2.4 m). This corresponded to a shoaling of $Z_{10\%}$ by 13–45% due to terrigenous CDOM (Fig. 8a,b). Even during the NE Monsoon, when the terrigenous CDOM concentration was lower than during the SW Monsoon, $Z_{10\%}$ shoaled by up to 1.9 m, or 17%. Across all seasons and sites, the percentage shoaling of $Z_{10\%}$ was related to the terrigenous CDOM concentration (Fig. 8c), which shows that terrigenous CDOM had a large impact on the depth of underwater light penetration despite variation in the concentrations of suspended sediments and phytoplankton between sites and dates. We also repeated our calculation of the depth-averaged irradiance in a well-mixed water column (Eq. 7), but using the K_d spectra calculated without terrigenous CDOM (see Section 2.8). We found that without terrigenous CDOM, the wavelength of peak irradiance was on average nearly identical between seasons (531–534 nm), and that the blue-to-green

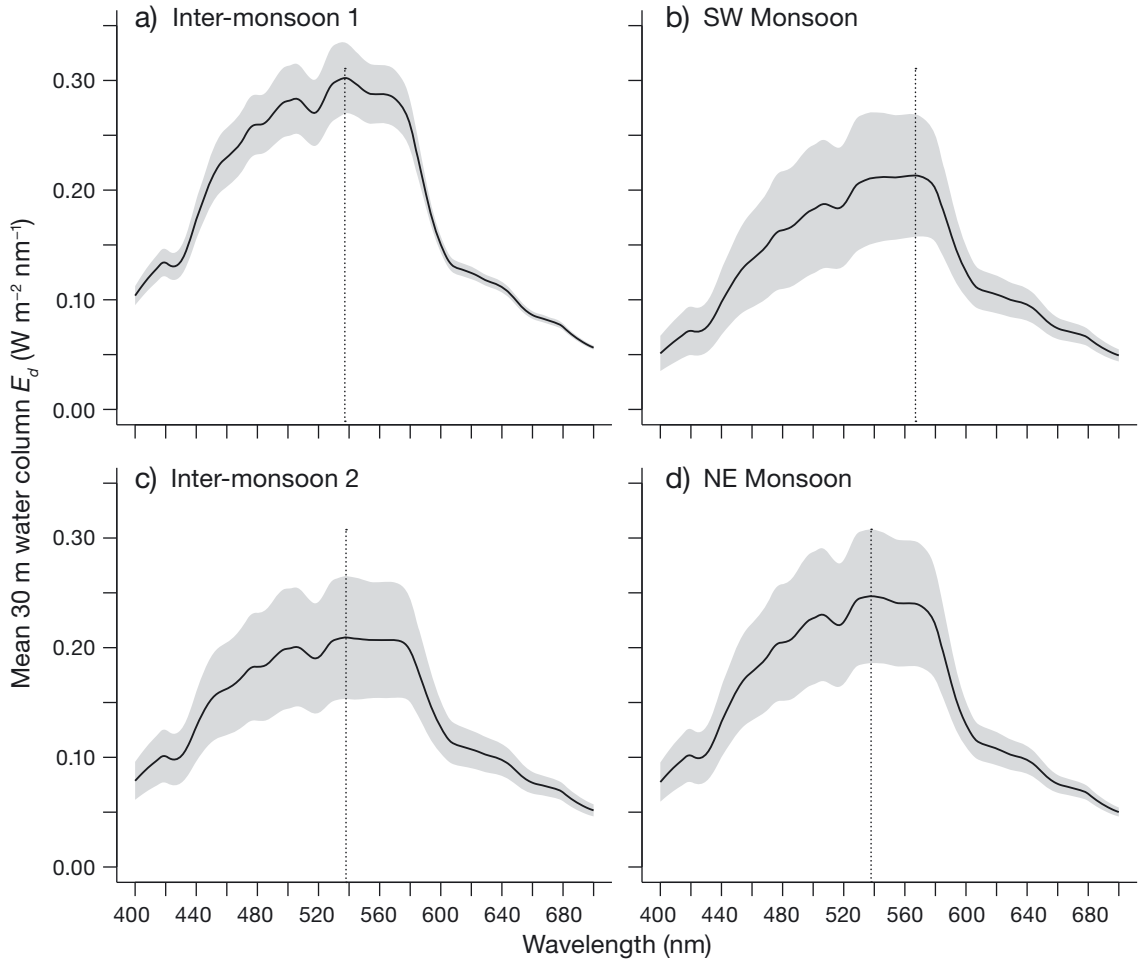

Fig. 6. Seasonal averages of depth-averaged downwelling irradiance at solar noon from 0 to 30 m, assuming turbulent mixing of the water column, for (a) March–May Inter-monsoon 1, (b) Southwest Monsoon, (c) September–November Inter-monsoon 2, and (d) Northeast Monsoon. Solid black line indicates the seasonal average irradiance spectrum, grey shading indicates ±1 SD. Vertical dotted lines indicate the wavelength of maximum irradiance

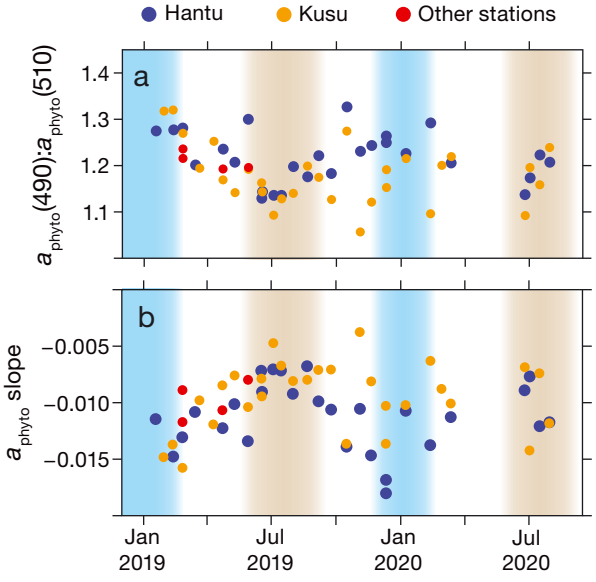

Fig. 7. Time series of (a) the ratio of phytoplankton absorption at 490 nm to phytoplankton absorption at 510 nm and (b) the phytoplankton absorption spectral slope (Eisner et al. 2003) both indicate that phytoplankton during the Southwest Monsoon have a lower proportion of non-photosynthetic to photosynthetic carotenoid pigments than during the other seasons (seasonal shading as in Fig. 2)

ratio $E_d(440):E_d(550)$ no longer showed significant seasonal differences (average of 0.59–0.62 for each season; Kruskal-Wallis test, χ^2 = 1.9, df = 3, p = 0.599).

To estimate how much of the observed shoaling of $Z_{10\%}$ might be the result of anthropogenic disturbance of peatlands, we repeated our calculations of K_d for the SW Monsoon but with the terrigenous CDOM absorption reduced by 35% of the observed value (see Section 2.8). We found that with only the

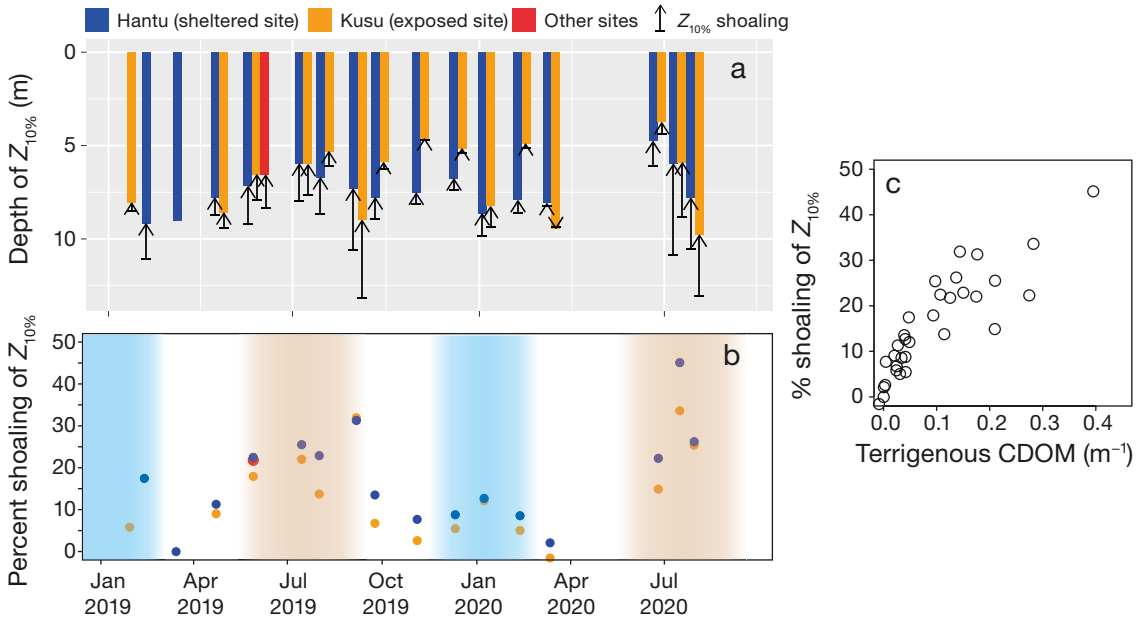

Fig. 8. Time-series data showing the impact of terrigenous coloured dissolved organic matter (CDOM) on the depth of 10% photosynthetically active radiation (PAR) penetration ($Z_{10\%}$). (a) Bars show the actually observed depth of $Z_{10\%}$, and arrows indicate by how much the depth of $Z_{10\%}$ was shoaled due to the presence of terrigenous CDOM (i.e. without terrigenous CDOM, $Z_{10\%}$ would extend to the bottom of the arrows). (b) Time series of the percentage reduction in $Z_{10\%}$ due to terrigenous CDOM. (seasonal shading as in Fig. 2). (c) Relationship between percentage reduction in $Z_{10\%}$ and the absorption coefficient at 440 nm by terrigenous CDOM

estimated natural fraction of terrigenous CDOM, $Z_{10\%}$ was on average 0.6 m deeper than the actual observed values (Table 1), while K_d(PAR) and K_d(500) would be lower on average by 0.028 and 0.033 m^{-1} (Table S1). This potentially anthropogenic contribution to light attenuation accounted for on average 25% of the observed $Z_{10\%}$ shoaling by terrigenous CDOM (Table 1).

Table 1. Estimated contribution to the shoaling of the depth of 10% photosynthetically active radiation (PAR) penetration ($Z_{10\%}$) by terrigenous coloured dissolved organic matter (CDOM) released by land-conversion of peatlands. Because our sites only receive peatland-derived CDOM during the Southwest Monsoon, this estimate was only made for measurements collected during this season. The percentage anthropogenic shoaling was calculated relative to the amount of shoaling caused by the total observed terrigenous CDOM. The anthropogenic terrigenous CDOM fraction was estimated as 35% of observed terrigenous CDOM, based on previous work (Moore et al. 2013, Yupi et al. 2016)

Date (yr-mo-d)	Site	Latitude (°N)	Longitude (°E)	Anthropogenic CDOM shoaling effect	
				$Z_{10\%}$ reduction (m)	Contribution to total (%)
2019-05-29	Hantu	1.227	103.746	0.56	27.2
2019-05-29	Kusu	1.226	103.860	0.40	28.1
2019-05-29	Other	1.246	103.738	0.48	26.4
2019-07-15	Hantu	1.227	103.746	0.50	24.4
2019-07-15	Kusu	1.226	103.860	0.45	26.3
2019-08-01	Hantu	1.227	103.746	0.52	26.3
2019-08-01	Kusu	1.226	103.860	0.24	27.9
2019-09-06	Hantu	1.227	103.746	0.79	23.7
2019-09-06	Kusu	1.226	103.860	1.00	23.8
2020-06-25	Hantu	1.227	103.746	0.33	24.1
2020-06-25	Kusu	1.226	103.860	0.18	27.1
2020-07-16	Hantu	1.227	103.746	0.89	18.2
2020-07-16	Kusu	1.226	103.860	0.65	21.9
2020-07-30	Hantu	1.227	103.746	0.71	25.6
2020-07-30	Kusu	1.226	103.860	0.87	26.1

4. DISCUSSION

4.1. Sources and seasonality of CDOM

Our time-series data showed significantly correlated seasonal variation in CDOM absorption, markers of CDOM terrestrial origin ($S_{275–295}$, S_R, and $SUVA_{254}$), and salinity. Moreover, the variability in CDOM across all seasons followed a pattern that is consistent with simple conservative mixing between 2 CDOM end-members (Fig. 3), where one has high a_{CDOM} and $SUVA_{254}$ with low $S_{275–295}$ and S_R (SW Monsoon), and the other has low a_{CDOM} and $SUVA_{254}$ with high $S_{275\text{-}295}$ and S_R (Inter-monsoon 1). $S_{275–295}$, S_R, and $SUVA_{254}$ are well established as accurate markers of terrigenous CDOM in regions receiving terrestrial inputs (Helms et al. 2008, Fichot & Benner 2012, Dainard & Guéguen 2013, Lu et al. 2016, Medeiros et al. 2017, Martin et al. 2018, Painter et al. 2018, Anderson et al. 2019, Carr et al. 2019). The ranges in these parameters that we observed during the SW Monsoon ($S_{275–295}$ mostly 0.015–0.020; S_R mostly 1.0–1.3; $SUVA_{254}$ mostly 1.5–3.0; Fig. 2) also match those from tropical peatland-draining river estuaries on Borneo (Martin et al. 2018). Together with the correlated changes in $SUVA_{254}$, our data therefore show that the Singapore Strait receives a large input of terrigenous CDOM that is aromatic-rich and has high apparent molecular weight during the SW Monsoon, and a smaller input of terrigenous CDOM during the NE Monsoon (Fig. 2). In contrast, the CDOM pool during the inter-monsoon seasons appears to be characterised by low apparent molecular weight and low aromaticity, consistent with a primarily marine, autochthonous source of CDOM such as from planktonic production (Fig. 2). Importantly, our data show that the seasonal changes in CDOM absorption can be largely explained by conservative mixing of the inter-monsoon marine CDOM with terrigenous CDOM delivered during the monsoons (Fig. 3). This justifies our interpretation that CDOM in the Singapore Strait is composed of a relatively constant and low background level of marine CDOM with a seasonally variable admixture of terrigenous CDOM.

In a separate analysis of the carbon biogeochemistry from our time series, Zhou et al. (2021) showed that the stable carbon isotope composition of DOC ($\delta^{13}C_{DOC}$) was as low as −25.5‰ during the SW Monsoon, which can only be explained by tDOC input. An isotope mass balance of dissolved organic and inorganic C showed that the riverine tDOC source during the SW Monsoon must have a mean (±SE) DOC concentration of 892 ± 104 µmol l^{-1} (Zhou et al. 2021). This is equal to the discharge-weighted mean (±SD) DOC concentration reported by Wit et al. (2018) for the 4 main peatland-draining river systems on Sumatra that are closest to our site (890 ± 159 µmol l^{-1}), which demonstrates that the tDOC and the terrigenous CDOM in the Singapore Strait during the SW Monsoon must originate from these peatlands. This is consistent with satellite remote sensing data that show CDOM spreading from Sumatra into the Malacca and Karimata Straits (Siegel et al. 2019). Although the smaller input of terrigenous CDOM during the NE Monsoon follows the same theoretical mixing line as the data from the SW Monsoon (Fig. 3), the differences in ocean currents obviously rule out Sumatran peatlands as the source of this CDOM. The terrigenous CDOM during the NE Monsoon might be derived largely from river input along the east coast of the Malay Peninsula (Kuwahara et al. 2010, Mizubayashi et al. 2013), which mostly consists of mineral soils rather than peatlands (Fig. 1).

In contrast, the $\delta^{13}C_{DOC}$ in the Singapore Strait during the late NE Monsoon and Inter-monsoon 1 averaged −22‰, consistent with a DOC pool that is fully of marine origin (Zhou et al. 2021). The relatively high salinity during the inter-monsoon seasons (up to 33) is close to typical values for the central South China Sea, which are mostly <34 (Wong et al. 2007), indicating that freshwater input (and therefore the potential for terrigenous CDOM input) is small outside of the SW and NE Monsoons. Because terrigenous CDOM in Southeast Asia also appears to be readily photo-bleachable (Martin et al. 2018, Zhou et al. 2021), terrigenous CDOM delivered to the Singapore Strait during the NE Monsoon is likely to be removed by photo-bleaching during Inter-monsoon 1. Photo-bleaching of terrigenous CDOM typically increases $S_{275–295}$ and S_R while lowering $SUVA_{254}$ (Helms et al. 2008, Martin et al. 2018; the seasonal changes that we observed would thus be consistent with photo-bleaching removing some terrigenous CDOM (Fig. 2).

The fact that chl *a* concentrations did not vary seasonally and were overall relatively low for a coastal environment further indicates that production of autochthonous, marine CDOM is unlikely to show strong seasonal variation (note that benthic communities such as coral reefs and seagrasses only cover small areas of the Singapore Strait [Tan et al. 2016], and are hence very unlikely to be quantitatively significant sources of autochthonous CDOM). The close similarity in the values of $a_{CDOM}(440)$ between the inter-monsoon months in all 3 years (2018–2020;

Fig. S4) provides additional evidence at interannual time scales that the background level of marine CDOM does not vary strongly over time in the Singapore Strait.

4.2. Impact of terrigenous CDOM on light availability

The rapid light attenuation, and resulting shallow $Z_{10\%}$ depth that we observed in our time series is consistent with previous data on vertical attenuation of PAR in the Singapore Strait (Chow et al. 2019, Morgan et al. 2020). Our data additionally show that the seasonal input of terrigenous CDOM to the Singapore Strait contributes significantly to the extinction of PAR with depth, and also alters the spectral quality of the available light (Figs. 4 & 5). This was already evident when just comparing the seasonal averages of $Z_{10\%}$, which varied by 2.0 m, even though the observed $Z_{10\%}$ was also clearly affected by the variability in particulate absorption and backscattering. After first estimating the fraction of CDOM that was terrigenous, we could quantify its impact directly by calculating hypothetically how the spectrum of K_d would differ in its absence; this showed that the advection of terrigenous CDOM during both monsoon seasons leads to shoaling of $Z_{10\%}$ by up to 45% (Fig. 8). Moreover, this shoaling was accompanied by spectral shifts in underwater irradiance, leading to less blue light and an irradiance peak shifted towards longer wavelengths (Figs. 5 & 6).

This result is consistent with the known importance of CDOM in reducing light penetration and altering the spectral quality of light in coastal waters (DeGrandpre et al. 1996, Foden et al. 2008, Mascarenhas et al. 2017). In coral reefs specifically, CDOM exerts a major control over the attenuation of UV radiation (Dunne & Brown 1996, Otis et al. 2004, Zepp et al. 2008), and reefs off Peninsular Malaysia have been shown to receive significant inputs of terrigenous CDOM (Kuwahara et al. 2010, Bowers et al. 2012). Mizubayashi et al. (2013) further showed that this terrigenous CDOM input is correlated with changes in UV and PAR attenuation ratios off northeastern Malaysia. Our data thus provide further evidence of the importance of CDOM in affecting the light environment of coral reefs, and also demonstrate that the spectral distribution of PAR is impacted (Fig. 5).

Our results also provide further support for the use of CDOM spectral slope measurements, especially $S_{275–295}$, to distinguish between marine and terrigenous CDOM in coastal waters (Stedmon & Markager 2001, Helms et al. 2008, Astoreca et al. 2009, Dainard & Guéguen 2013, Vantrepotte et al. 2015, Lu et al. 2016). Such a partitioning between marine and terrigenous CDOM fractions and their respective contributions to the spectral light attenuation in coastal waters is needed for a better understanding of the potential drivers of light availability in shelf seas.

We infer that around 25% of the seasonal CDOM-mediated shoaling of $Z_{10\%}$ might be an anthropogenic effect caused by increased tDOC flux after peatland disturbance (Moore et al. 2013, Yupi et al. 2016). Although it has been well documented that the CDOM pool in shelf seas can contain a large fraction of terrigenous CDOM (Blough et al. 1993, Stedmon et al. 2010, Mizubayashi et al. 2013, Carr et al. 2019), the long-term dynamics and potential anthropogenic drivers of terrigenous CDOM in coastal waters remain poorly known. So far, there is only limited and mostly indirect evidence that anthropogenic increases in coastal CDOM concentrations have occurred and reduced light penetration, and this has only been reported off southern Norway (Aksnes et al. 2009, Frigstad et al. 2013) and in the Gulf of Maine (Balch et al. 2016). The potential anthropogenic contribution to the seasonal shoaling of $Z_{10\%}$ that we infer (mean of 0.6 m and up to 1.0 m; Table 1) is similar in magnitude to the long-term changes in Secchi depth reported for the Baltic Sea (long-term decrease of 3.2 m) and the North Sea (long-term decrease of 1.8 m) in waters shallower than 100 m (Dupont & Aksnes 2013). The potential anthropogenic increases in K_d(PAR) and in K_d(500) that we estimated (Table S1) are also slightly higher than the long-term increase in K_d(500) of 0.022 m^{-1} reported by Aksnes et al. (2009) in Norwegian coastal waters, but slightly lower than the centennial changes in non-phytoplankton K_d(PAR) estimated by Opdal et al. (2019) for the North Sea (0.08–0.15 m^{-1}). However, the estimates by Opdal et al. (2019) and by Dupont & Aksnes (2013) likely include contributions from suspended particles, and not just CDOM. Overall, the potential increase in light attenuation due to anthropogenic CDOM that we report here appears to be comparable in magnitude to previous reports.

Our estimate of the anthropogenic contribution to the observed CDOM-mediated light attenuation relies on earlier reports that the peatland tDOC flux has increased by roughly 50% due to land conversion (Moore et al. 2013, Yupi et al. 2016). Future research needs to corroborate our estimate by reconstructing past variation in terrigenous CDOM in this region, e.g. using luminescence data from coral

skeleton cores as a terrigenous CDOM palaeo-proxy (Kaushal et al. 2020, 2021). Nevertheless, our study already indicates that the disturbance of tropical peatlands has likely resulted in CDOM-mediated coastal browning in Southeast Asia, and that peatland disturbance therefore entails an additional environmental impact beyond the large increases in CO_2 emissions from peat and peatland DOC oxidation (Hooijer et al. 2010, Murdiyarso et al. 2010, Wit et al. 2018).

4.3. Ecological implications

Primary production by benthic communities and by phytoplankton requires sufficient light availability, and rapid vertical extinction of PAR can therefore limit planktonic and benthic primary productivity, and restrict the depth to which photosynthetic benthic communities can occur (Gattuso et al. 2006). In this section, we will first discuss the implications of our results for phytoplankton, and then for benthic communities.

Our estimates of the depth-averaged underwater irradiance in a turbulent water column show that phytoplankton in the Singapore Strait are subject to seasonal changes in intensity and spectral composition of irradiance (Fig. 6). The fact that the phytoplankton absorption spectral slope increased and the $a_{phyto}(490):a_{phyto}(510)$ ratio decreased during the SW Monsoon suggests that the phytoplankton adapted their pigment composition in response to the CDOM-driven changes in the light environment. Specifically, the observed changes indicate a higher ratio of photoprotective to photosynthetic carotenoid pigments during both inter-monsoons, and a lower ratio during the SW Monsoon (Eisner et al. 2003, Hickman et al. 2009). Because the phytoplankton community in the Singapore Strait does not undergo large seasonal changes (Gin et al. 2000, Chénard et al. 2019), our data most likely reflect phytoplankton photo-acclimation rather than a taxonomic community shift. Such chromatic adaptation by marine phytoplankton occurs in response to variation in the light environment (Hickman et al. 2009, Isada et al. 2013, Pérez et al. 2021). Whether the changes we observed in the a_{phyto} spectra were driven more by the seasonal change in spectral light quality or more by the reduction in total light intensity is unclear, but they suggest that the seasonal change in light availability caused by peatland CDOM was sufficiently large to drive changes in phytoplankton pigment composition. Lower light availability during the SW Monsoon may be a reason why the chl *a* concentration remains relatively constant (Fig. S6) despite increases in nutrient concentrations during this season by 3–5 µmol l^{-1} dissolved inorganic nitrogen and 0.3–0.4 µmol l^{-1} dissolved inorganic phosphorus (Chénard et al. 2019).

Our data also show that benthic communities in the Singapore Strait are exposed to seasonal changes both in total PAR intensity and in spectral quality of irradiance (Figs. 5 & 8). The Singapore Strait is home to >100 different scleractinian coral species, as well as seagrass meadows and macroalgae, but the depth range of these photosynthetic benthic communities is restricted to the upper 10 m (Huang et al. 2009, McKenzie et al. 2016, Low et al. 2019). This shallow depth limit is attributed to a combination of sediment stress and light limitation at deeper depths (Guest et al. 2016, McKenzie et al. 2016, Chow et al. 2019, Morgan et al. 2020), and matches quite closely the average $Z_{10\%}$ of around 7 m that we measured. Coral reef monitoring data suggest that coral cover at depths of 6–7 m (but not at 3–4 m) has decreased since the 1980s (Guest et al. 2016), probably as a result of both sedimentation and light limitation (Morgan et al. 2020).

It has been suggested that coral communities in shallow, low-light environments such as the Singapore Strait should be considered as mesophotic coral ecosystems, analogous to those found below 30–40 m depth in clear, 'blue-water' environments (Laverick et al. 2020, Morgan et al. 2020). Although these systems show many ecological similarities, e.g. in species composition (Eyal et al. 2016, Chow et al. 2019, Laverick et al. 2020), the spectral distribution of the available light in the Singapore Strait is clearly very different compared to deep mesophotic ecosystems that receive mostly blue wavelengths (Kahng et al. 2019). It is possible that such differences in spectral light quality might be physiologically and ecologically significant for coral reefs. Corals clearly acclimate to low light intensities (Kahng et al. 2019), such as by altering their skeletal morphology to minimise self-shading (Todd 2008, Ow & Todd 2010), and by enhancing light scattering by the skeleton and light absorption within the tissue layer (Polinski & Voss 2018, Kramer et al. preprint doi:10.1101/2020.12.04.411496). However, spectral light quality also affects coral physiology, and numerous studies have demonstrated that blue light appears to be particularly important at controlling coral physiological rates (Kinzie & Hunter 1987, Mass et al. 2010, Cohen et al. 2016), while red light was found to reduce the health and survival of *Stylophora pistillata* (Wijgerde et al. 2014). Blue light also controls the fluorescent pigmentation of several

coral taxa (D'Angelo et al. 2008). Although it is still debated whether fluorescent proteins play a photophysiological role in enabling coral acclimation to low-intensity blue light (D'Angelo et al. 2008, Roth et al. 2015, Kahng et al. 2019), Smith et al. (2017) showed that the presence of a fluorescent protein was necessary for long-term survival of 2 coral species under low-intensity blue light. If the availability of blue light is indeed ecologically important for corals, it is possible that the spectral differences in irradiance between shallow and deep mesophotic systems might play a role in controlling factors such as the lower depth limit of coral growth or the coral species community composition. If spectral differences in irradiance influence coral photosynthetic rates, shallow mesophotic conditions might also require corals to rely to a greater extent on heterotrophic nutrition (Anthony & Fabricius 2000).

The decline in coral cover at 6–7 m in the Singapore Strait since the 1980s reported by Guest et al. (2016) was originally attributed to possible increases in suspended sediments and sedimentation. However, this period of coral cover loss at deeper sites also coincides with the major period of land conversion of peatlands across Southeast Asia (Miettinen et al. 2016). Our results indicate that if peatland disturbance has indeed increased tDOC fluxes by as much as currently thought, then the associated reduction in light transmission due to terrigenous CDOM has likely contributed to these benthic cover changes.

4.4. Conclusions

Our data demonstrate the importance of terrigenous CDOM for the optical properties of peatland-influenced areas of the Sunda Shelf Sea, and show further that the seasonal, monsoon-driven advection of this terrigenous CDOM drives significant variation in the transmission and spectral quality of light underwater. We also observed seasonal variation in phytoplankton absorption properties that are indicative of changes in photo-acclimation, which suggests that this variation in light attenuation was ecologically relevant. Moreover, our study suggests that land conversion in the tropics has the potential to cause CDOM-mediated coastal browning in biologically diverse shelf-sea environments, which may have contributed to observed coral-cover decline. Overall, our study underscores the importance of examining not only biogeochemical impacts of land–ocean tDOC fluxes, but also the consequences for optical water quality due to the associated terrigenous CDOM.

Data availability. The final dataset used in this study, all data analysis codes, and all raw data are available via the NTU Data Repository under doi:10.21979/N9/TXYRC3. A preprint of this article is available at BioRxiv doi:10.1101/2021.03.30.437655.

Acknowledgements. Yongli Zhou, Chen Shuang, Nikita Kaushal, Molly Moynihan, Rob Nichols, Tan Li, Daniel Kalbermatter, Jervis Ong Zhe Ao, Lee Tian Li, Phyllis Kho Yu Yi, Kyle Morgan, Woo Oon Yee, and Chen Yuan assisted with fieldwork and laboratory analyses. We thank Sapari, Surpato, and Francis Yeo of 'Dolphin Explorer' for enabling the sample collection. Comments by Richard Sanders, Adam Switzer, and 3 anonymous reviewers improved this manuscript. Field work was carried out under permit NP/RP17-044-2 from the Singapore National Parks Board. This research was supported by the National Research Foundation Singapore, Prime Minister's Office, under the Marine Science Research and Development Program through grant MSRDP-P32 to P.M.

LITERATURE CITED

Aksnes DL, Dupont N, Staby A, Fiksen Ø, Kaartvedt S, Aure J (2009) Coastal water darkening and implications for mesopelagic regime shifts in Norwegian fjords. Mar Ecol Prog Ser 387:39–49

Anderson TR, Rowe EC, Polimene L, Tipping E and others (2019) Unified concepts for understanding and modelling turnover of dissolved organic matter from freshwaters to the ocean: the UniDOM model. Biogeochemistry 146:105–123

Anthony KRN, Fabricius KE (2000) Shifting roles of heterotrophy and autotrophy in coral energetics under varying turbidity. J Exp Mar Biol Ecol 252:221–253

Arrigo KR, Brown CW (1996) Impact of chromophoric dissolved organic matter on UV inhibition of primary productivity in the sea. Mar Ecol Prog Ser 140:207–216

Ask J, Karlsson J, Persson L, Ask P, Byström P, Jansson M (2009) Terrestrial organic matter and light penetration: effects on bacterial and primary production in lakes. Limnol Oceanogr 54:2034–2040

Astoreca R, Rousseau V, Lancelot C (2009) Coloured dissolved organic matter (CDOM) in southern North Sea waters: optical characterization and possible origin. Estuar Coast Shelf Sci 85:633–640

Balch WM, Drapeau DT, Bowler BC, Huntington TG (2012) Step-changes in the physical, chemical and biological characteristics of the Gulf of Maine, as documented by the GNATS time series. Mar Ecol Prog Ser 450:11–35

Balch W, Huntington T, Aiken G, Drapeau D, Bowler B, Lubelczyk L, Butler K (2016) Toward a quantitative and empirical dissolved organic carbon budget for the Gulf of Maine, a semienclosed shelf sea. Global Biogeochem Cycles 30:268–292

Banaszak AT, Lesser MP (2009) Effects of solar ultraviolet radiation on coral reef organisms. Photochem Photobiol Sci 8:1276–1294

Baum A, Rixen T, Samiaji J (2007) Relevance of peat draining rivers in central Sumatra for the riverine input of dissolved organic carbon into the ocean. Estuar Coast Shelf Sci 73:563–570

Beleites C, Sergo V (2018) hyperSpec: a package to handle hyperspectral data sets in R. http://hyperspec.r-forge.r-project.org

Blough NV, Zafiriou OC, Bonilla J (1993) Optical absorption spectra of waters from the Orinoco River outflow: terrestrial input of colored organic matter to the Caribbean. J Geophys Res Oceans 98:2271–2278

Boss E, Pegau WS (2001) Relationship of light scattering at an angle in the backward direction to the backscattering coefficient. Appl Opt 40:5503–5507

Bowers DG, Md-Suffian I, Mitchelson-Jacob EG (2012) Bio-optical properties of east coast Malaysia waters in relation to remote sensing of chlorophyll. Int J Remote Sens 33:150–169

Burkholder JM, Tomasko DA, Touchette BW (2007) Seagrasses and eutrophication. J Exp Mar Biol Ecol 350:46–72

Carr N, Davis CE, Blackbird S, Daniels LR, Preece C, Woodward M, Mahaffey C (2019) Seasonal and spatial variability in the optical characteristics of DOM in a temperate shelf sea. Prog Oceanogr 177:101929

Chan ES, Tkalich P, Gin KYH, Obbard JP (2006) The physical oceanography of Singapore coastal waters and its implications for oil spills. In: Wolanski E (ed) The environment in Asia Pacific harbours. Springer Netherlands, Dordrecht, p 393–412

Chen Z, Doering PH, Ashton M, Orlando BA (2015) Mixing behavior of colored dissolved organic matter and its potential ecological implication in the Caloosahatchee River Estuary, Florida. Estuaries Coasts 38:1706–1718

Chénard C, Wijaya W, Vaulot D, Lopes dos Santos A, Martin P, Kaur A, Lauro FM (2019) Temporal and spatial dynamics of *Bacteria*, *Archaea* and protists in equatorial coastal waters. Sci Rep 9:16390

Cherukuru N, Brando VE, Schroeder T, Clementson LA, Dekker AG (2014) Influence of river discharge and ocean currents on coastal optical properties. Cont Shelf Res 84: 188–203

Chow GSE, Chan YKS, Jain SS, Huang D (2019) Light limitation selects for depth generalists in urbanised reef coral communities. Mar Environ Res 147:101–112

Coble PG (2007) Marine optical biogeochemistry: the chemistry of ocean color. Chem Rev 107:402–418

Cohen I, Dubinsky Z, Erez J (2016) Light enhanced calcification in hermatypic corals: new insights from light spectral responses. Front Mar Sci 2:122

Cook S, Peacock M, Evans CD, Page SE, Whelan MJ, Gauci V, Kho LK (2017) Quantifying tropical peatland dissolved organic carbon (DOC) using UV-visible spectroscopy. Water Res 115:229–235

Costanza R, de Groot R, Sutton P, van der Ploeg S and others (2014) Changes in the global value of ecosystem services. Glob Environ Change 26:152–158

D'Angelo C, Denzel A, Vogt A, Matz MV and others (2008) Blue light regulation of host pigment in reef-building corals. Mar Ecol Prog Ser 364:97–106

Dainard PG, Guéguen C (2013) Distribution of PARAFAC modeled CDOM components in the North Pacific Ocean, Bering, Chukchi and Beaufort Seas. Mar Chem 157: 216–223

de Wit HA, Valinia S, Weyhenmeyer GA, Futter MN and others (2016) Current browning of surface waters will be further promoted by wetter climate. Environ Sci Technol Lett 3:430–435

DeGrandpre MD, Vodacek A, Nelson RK, Bruce EJ, Blough NV (1996) Seasonal seawater optical properties of the US Middle Atlantic Bight. J Geophys Res Oceans 101: 22727–22736

Dennison WC, Orth RJ, Moore KA, Stevenson JC and others (1993) Assessing water quality with submersed aquatic vegetation: habitat requirements as barometers of Chesapeake Bay health. Bioscience 43:86–94

Duarte CM (1995) Submerged aquatic vegetation in relation to different nutrient regimes. Ophelia 41:87–112

Dunne RP, Brown BE (1996) Penetration of solar UVB radiation in shallow tropical waters and its potential biological effects on coral reefs; results from the central Indian Ocean and Andaman Sea. Mar Ecol Prog Ser 144:109–118

Dupont N, Aksnes DL (2013) Centennial changes in water clarity of the Baltic Sea and the North Sea. Estuar Coast Shelf Sci 131:282–289

Edmunds PJ, Tsounis G, Boulon R, Bramanti L (2018) Long-term variation in light intensity on a coral reef. Coral Reefs 37:955–965

Eisner LB, Twardowski MS, Cowles TJ, Perry MJ (2003) Resolving phytoplankton photoprotective:photosynthetic carotenoid ratios on fine scales using *in situ* spectral absorption measurements. Limnol Oceanogr 48:632–646

Evans CD, Monteith DT, Cooper DM (2005) Long-term increases in surface water dissolved organic carbon: observations, possible causes and environmental impacts. Environ Pollut 137:55–71

Evans CD, Chapman PJ, Clark JM, Monteith DT, Cresser MS (2006) Alternative explanations for rising dissolved organic carbon export from organic soils. Glob Change Biol 12:2044–2053

Eyal G, Eyal-Shaham L, Cohen I, Tamir R, Ben-Zvi O, Sinniger F, Loya Y (2016) *Euphyllia paradivisa*, a successful mesophotic coral in the northern Gulf of Eilat/Aqaba, Red Sea. Coral Reefs 35:91–102

Fabricius KE (2005) Effects of terrestrial runoff on the ecology of corals and coral reefs: review and synthesis. Mar Pollut Bull 50:125–146

Ferrari GM, Tassan S (1999) A method using chemical oxidation to remove light absorption by phytoplankton pigments. J Phycol 35:1090–1098

Ferrero E, Eöry M, Ferreyra G, Schloss I, Zagarese H, Vernet M, Momo F (2006) Vertical mixing and ecological effects of ultraviolet radiation in planktonic communities. Photochem Photobiol 82:898–902

Fichot CG, Benner R (2011) A novel method to estimate DOC concentrations from CDOM absorption coefficients in coastal waters. Geophys Res Lett 38:L03610

Fichot CG, Benner R (2012) The spectral slope coefficient of chromophoric dissolved organic matter ($S_{275–295}$) as a tracer of terrigenous dissolved organic carbon in river-influenced ocean margins. Limnol Oceanogr 57: 1453–1466

Fichot CG, Kaiser K, Hooker SB, Amon RMW and others (2013) Pan-Arctic distributions of continental runoff in the Arctic Ocean. Sci Rep 3:1053

Fichot CG, Lohrenz SE, Benner R (2014) Pulsed, cross-shelf export of terrigenous dissolved organic carbon to the Gulf of Mexico. J Geophys Res Oceans 119:1176–1194

Filbee-Dexter K, Wernberg T (2018) Rise of turfs: a new battlefront for globally declining kelp forests. Bioscience 68:64–76

Foden J, Sivyer DB, Mills DK, Devlin MJ (2008) Spatial and temporal distribution of chromophoric dissolved organic matter (CDOM) fluorescence and its contribution to light attenuation in UK waterbodies. Estuar Coast Shelf Sci 79:707–717

Frigstad H, Andersen T, Hessen DO, Jeansson E and others (2013) Long-term trends in carbon, nutrients and stoi-

chiometry in Norwegian coastal waters: evidence of a regime shift. Prog Oceanogr 111:113–124
Gattuso JP, Gentili B, Duarte CM, Kleypas JA, Middelburg JJ, Antoine D (2006) Light availability in the coastal ocean: impact on the distribution of benthic photosynthetic organisms and their contribution to primary production. Biogeosciences 3:489–513
Gerea M, Pérez GL, Unrein F, Soto Cárdenas C, Morris D, Queimaliños C (2017) CDOM and the underwater light climate in two shallow North Patagonian lakes: evaluating the effects on nano and microphytoplankton community structure. Aquat Sci 79:231–248
Gin KYH, Lin X, Zhang S (2000) Dynamics and size structure of phytoplankton in the coastal waters of Singapore. J Plankton Res 22:1465–1484
Graneli W (2012) Brownification of lakes. In: Bengtsson L, Herschy RW, Fairbridge RW (eds) Encyclopedia of lakes and reservoirs. Springer Netherlands, Dordrecht, p 117–119
Green SA, Blough NV (1994) Optical absorption and fluorescence properties of chromophoric dissolved organic matter in natural waters. Limnol Oceanogr 39:1903–1916
Guest JR, Tun K, Low J, Vergés A and others (2016) 27 years of benthic and coral community dynamics on turbid, highly urbanised reefs off Singapore. Sci Rep 6:36260
Häder DP, Williamson CE, Wängberg SÅ, Rautio M and others (2015) Effects of UV radiation on aquatic ecosystems and interactions with other environmental factors. Photochem Photobiol Sci 14:108–126
Hamzah F, Agustiadi T, Susanto RD, Wei Z, Guo L, Cao Z, Dai M (2020) Dynamics of the carbonate system in the western Indonesian seas during the Southeast Monsoon. J Geophys Res Oceans 125:e2018JC014912
Heery EC, Hoeksema BW, Browne NK, Reimer JD and others (2018) Urban coral reefs: degradation and resilience of hard coral assemblages in coastal cities of East and Southeast Asia. Mar Pollut Bull 135:654–681
Helms JR, Stubbins A, Ritchie JD, Minor EC, Kieber DJ, Mopper K (2008) Absorption spectral slopes and slope ratios as indicators of molecular weight, source, and photobleaching of chromophoric dissolved organic matter. Limnol Oceanogr 53:955–969
Hessen DO, Carroll J, Kjeldstad B, Korosov AA, Pettersson LH, Pozdnyakov D, Sørensen K (2010) Input of organic carbon as determinant of nutrient fluxes, light climate and productivity in the Ob and Yenisey estuaries. Estuar Coast Shelf Sci 88:53–62
Hickman AE, Holligan PM, Moore CM, Sharples J, Krivtsov V, Palmer MR (2009) Distribution and chromatic adaptation of phytoplankton within a shelf sea thermocline. Limnol Oceanogr 54:525–536
Hooijer A, Page S, Canadell JG, Silvius M, Kwadijk J, Wösten H, Jauhiainen J (2010) Current and future CO_2 emissions from drained peatlands in Southeast Asia. Biogeosciences 7:1505–1514
Huang D, Tun KPP, Chou LM, Todd PA (2009) An inventory of zooxanthellate scleractinian corals in Singapore, including 33 new records. Raffles Bull Zool 22:69–80
IOCCG (2000) Remote sensing of ocean colour in coastal, and other optically-complex, waters. Reports of the International Ocean-Colour Coordinating Group 3. IOCCG, Dartmouth
Isada T, Iida T, Liu H, Saitoh SI, Nishioka J, Nakatsuka T, Suzuki K (2013) Influence of Amur River discharge on phytoplankton photophysiology in the Sea of Okhotsk during late summer. J Geophys Res Oceans 118: 1995–2013
Kahng SE, Akkaynak D, Shlesinger T, Hochberg EJ, Wiedenmann J, Tamir R, Tchernov D (2019) Light, temperature, photosynthesis, heterotrophy, and the lower depth limits of mesophotic coral ecosystems. In: Loya Y, Puglise KA, Bridge TCL (eds) Mesophotic coral ecosystems. Springer International Publishing, Cham, p 801–828
Kaiser K, Benner R, Amon RMW (2017) The fate of terrigenous dissolved organic carbon on the Eurasian shelves and export to the North Atlantic. J Geophys Res Oceans 122:4–22
Kaushal N, Yang L, Tanzil JTI, Lee JN, Goodkin NF, Martin P (2020) Sub-annual fluorescence measurements of coral skeleton: relationship between skeletal luminescence and terrestrial humic-like substances. Coral Reefs 39: 1257–1272
Kaushal N, Sanwlani N, Tanzil JTI, Cherukuru N and others (2021) Coral skeletal luminescence records changes in terrestrial chromophoric dissolved organic matter (CDOM) in tropical coastal waters. Geophys Res Lett 48: e2020GL092130
Kinzie RA, Hunter T (1987) Effect of light quality on photosynthesis of the reef coral *Montipora verrucosa*. Mar Biol 94:95–109
Kirk JTO (1988) Optical water quality: What does it mean and how should we measure it? J Water Pollut Control Fed 60:194–197
Kjeldstad B, Frette Ø, Erga SR, Browman HI and others (2003) UV (280 to 400 nm) optical properties in a Norwegian fjord system and an intercomparison of underwater radiometers. Mar Ecol Prog Ser 256:1–11
Kowalczuk P, Olszewski J, Darecki M, Kaczmarek S (2005) Empirical relationships between coloured dissolved organic matter (CDOM) absorption and apparent optical properties in Baltic Sea waters. Int J Remote Sens 26: 345–370
Kowalczuk PA, Stedmon CA, Markager S (2006) Modeling absorption by CDOM in the Baltic Sea from season, salinity and chlorophyll. Mar Chem 101:1–11
Kuwahara VS, Nakajima R, Othman BHR, Kushairi MRM, Toda T (2010) Spatial variability of UVR attenuation and bio-optical factors in shallow coral-reef waters of Malaysia. Coral Reefs 29:693–704
Larsen S, Andersen TOM, Hessen DO (2011) Climate change predicted to cause severe increase of organic carbon in lakes. Glob Change Biol 17:1186–1192
Laverick JH, Tamir R, Eyal G, Loya Y (2020) A generalized light-driven model of community transitions along coral reef depth gradients. Glob Ecol Biogeogr 29:1554–1564
Lee Z (2009) K_{PAR}: an optical property associated with ambiguous values. Hupo Kexue 21:159–164
Lee ZP, Du KP, Arnone R (2005) A model for the diffuse attenuation coefficient of downwelling irradiance. J Geophys Res Oceans 110:C02016
Lee Z, Shang S, Du K, Wei J (2018) Resolving the long-standing puzzles about the observed Secchi depth relationships. Limnol Oceanogr 63:2321–2336
Lisovski S, Hahn S (2012) GeoLight — processing and analysing light-based geolocation in R. Methods Ecol Evol 3:1055–1059
Low JKY, Fong J, Todd PA, Chou LM, Bauman AG (2019) Seasonal variation of *Sargassum ilicifolium* (Phaeophyceae) growth on equatorial coral reefs. J Phycol 55: 289–296

Lu CJ, Benner R, Fichot CG, Fukuda H, Yamashita Y, Ogawa H (2016) Sources and transformations of dissolved lignin phenols and chromophoric dissolved organic matter in Otsuchi Bay, Japan. Front Mar Sci 3:85

Martin P, Cherukuru N, Tan ASY, Sanwlani N, Mujahid A, Müller M (2018) Distribution and cycling of terrigenous dissolved organic carbon in peatland-draining rivers and coastal waters of Sarawak, Borneo. Biogeosciences 15: 6847–6865

Mascarenhas VJ, Voß D, Wollschlaeger J, Zielinski O (2017) Fjord light regime: bio-optical variability, absorption budget, and hyperspectral light availability in Sognefjord and Trondheimsfjord, Norway. J Geophys Res Oceans 122:3828–3847

Mass T, Kline DI, Roopin M, Veal CJ, Cohen S, Iluz D, Levy O (2010) The spectral quality of light is a key driver of photosynthesis and photoadaptation in *Stylophora pistillata* colonies from different depths in the Red Sea. J Exp Biol 213:4084–4091

Massicotte P, Asmala E, Stedmon C, Markager S (2017) Global distribution of dissolved organic matter along the aquatic continuum: across rivers, lakes and oceans. Sci Total Environ 609:180–191

Mayer B, Pohlmann T (2014) Simulation of organic pollutants: first step towards an adaptation to the Malacca Strait. Asian J Water Environ Pollut 11:75–86

Mayer B, Stacke T, Stottmeister I, Pohlmann T (2015) Sunda Shelf Seas: flushing rates and residence times. Ocean Sci Discuss 12:863–895

Mayer B, Rixen T, Pohlmann T (2018) The spatial and temporal variability of air–sea CO_2 fluxes and the effect of net coral reef calcification in the Indonesian Seas: a numerical sensitivity study. Front Mar Sci 5:116

McKenzie LJ, Yaakub SM, Tan R, Seymour J, Yoshida RL (2016) Seagrass habitats of Singapore: environmental drivers and key processes. Raffles Bull Zool Suppl 34: 60–77

Medeiros PM, Babcock-Adams L, Seidel M, Castelao RM, Di Iorio D, Hollibaugh JT, Dittmar T (2017) Export of terrigenous dissolved organic matter in a broad continental shelf. Limnol Oceanogr 62:1718–1731

Miettinen J, Shi C, Liew SC (2016) Land cover distribution in the peatlands of Peninsular Malaysia, Sumatra and Borneo in 2015 with changes since 1990. Glob Ecol Conserv 6:67–78

Mizubayashi K, Kuwahara VS, Segaran TC, Zaleha K, Effendy AWM, Kushairi MRM, Toda T (2013) Monsoon variability of ultraviolet radiation (UVR) attenuation and bio-optical factors in the Asian tropical coral-reef waters. Estuar Coast Shelf Sci 126:34–43

Monteith DT, Stoddard JL, Evans CD, de Wit HA and others (2007) Dissolved organic carbon trends resulting from changes in atmospheric deposition chemistry. Nature 450:537–540

Moore S, Evans CD, Page SE, Garnett MH and others (2013) Deep instability of deforested tropical peatlands revealed by fluvial organic carbon fluxes. Nature 493:660–663

Morgan KM, Moynihan MA, Sanwlani N, Switzer AD (2020) Light limitation and depth-variable sedimentation drives vertical reef compression on turbid coral reefs. Front Mar Sci 7:571256

Murdiyarso D, Hergoualc'h K, Verchot LV (2010) Opportunities for reducing greenhouse gas emissions in tropical peatlands. Proc Natl Acad Sci USA 107:19655–19660

Noacco V, Wagener T, Worrall F, Burt TP, Howden NJK (2017) Human impact on long-term organic carbon export to rivers. J Geophys Res Biogeosci 122:947–965

Opdal AF, Lindemann C, Aksnes DL (2019) Centennial decline in North Sea water clarity causes strong delay in phytoplankton bloom timing. Glob Change Biol 25: 3946–3953

Osburn CL, Kinsey JD, Bianchi TS, Shields MR (2019) Formation of planktonic chromophoric dissolved organic matter in the ocean. Mar Chem 209:1–13

Otis DB, Carder KL, English DC, Ivey JE (2004) CDOM transport from the Bahamas Banks. Coral Reefs 23:152–160

Ow YX, Todd PA (2010) Light-induced morphological plasticity in the scleractinian coral *Goniastrea pectinata* and its functional significance. Coral Reefs 29:797–808

Painter SC, Lapworth DJ, Woodward EMS, Kroeger S, Evans CD, Mayor DJ, Sanders RJ (2018) Terrestrial dissolved organic matter distribution in the North Sea. Sci Total Environ 630:630–647

Pérez GL, Galí M, Royer SJ, Gerea M and others (2021) Variability of phytoplankton light absorption in stratified waters of the NW Mediterranean Sea: the interplay between pigment composition and the packaging effect. Deep-Sea Res I 169:103460

Petus C, Devlin M, Silva E, Lewis S and others (2018) Defining wet season water quality target concentrations for ecosystem conservation using empirical light attenuation models: a case study in the Great Barrier Reef (Australia). J Environ Manag 213:451–466

Polinski JM, Voss JD (2018) Evidence of photoacclimatization at mesophotic depths in the coral–*Symbiodinium* symbiosis at Flower Garden Banks National Marine Sanctuary and McGrail Bank. Coral Reefs 37:779–789

Pope RM, Fry ES (1997) Absorption spectrum (380–700 nm) of pure water. II. Integrating cavity measurements. Appl Opt 36:8710–8723

Roth MS, Padilla-Gamiño JL, Pochon X, Bidigare RR, Gates RD, Smith CM, Spalding HL (2015) Fluorescent proteins in dominant mesophotic reef-building corals. Mar Ecol Prog Ser 521:63–79

Siegel H, Gerth M, Stottmeister I, Baum A, Samiaji J (2019) Remote sensing of coastal discharge of SE Sumatra (Indonesia). In: Barale V, Gade M (eds) Remote sensing of the Asian Seas. Springer International Publishing, Cham, p 359–376

Signorini SR, Mannino A, Friedrichs MAM, St-Laurent P and others (2019) Estuarine dissolved organic carbon flux from space: with application to Chesapeake and Delaware Bays. J Geophys Res Oceans 124:3755–3778

Skjelkvåle BL, Stoddard JL, Jeffries DS, Tørseth K and others (2005) Regional scale evidence for improvements in surface water chemistry 1990–2001. Environ Pollut 137: 165–176

Smith EG, D'Angelo C, Sharon Y, Tchernov D, Wiedenmann J (2017) Acclimatization of symbiotic corals to mesophotic light environments through wavelength transformation by fluorescent protein pigments. Proc R Soc B 284:20170320

Smith RC, Baker KS (1981) Optical properties of the clearest natural waters (200–800 nm). Appl Opt 20:177–184

Solomon CT, Jones SE, Weidel BC, Buffam I and others (2015) Ecosystem consequences of changing inputs of terrestrial dissolved organic matter to lakes: current knowledge and future challenges. Ecosystems 18:376–389

Stedmon CA, Markager S (2001) The optics of chromophoric dissolved organic matter (CDOM) in the Greenland Sea: an algorithm for differentiation between marine and ter-

restrially derived organic matter. Limnol Oceanogr 46: 2087–2093
Stedmon CA, Markager S (2003) Behaviour of the optical properties of coloured dissolved organic matter under conservative mixing. Estuar Coast Shelf Sci 57:973–979
Stedmon CA, Osburn CL, Kragh T (2010) Tracing water mass mixing in the Baltic–North Sea transition zone using the optical properties of coloured dissolved organic matter. Estuar Coast Shelf Sci 87:156–162
Stomp M, Huisman J, Vörös L, Pick FR, Laamanen M, Haverkamp T, Stal LJ (2007) Colourful coexistence of red and green picocyanobacteria in lakes and seas. Ecol Lett 10:290–298
Storlazzi CD, Norris BK, Rosenberger KJ (2015) The influence of grain size, grain color, and suspended-sediment concentration on light attenuation: why fine-grained terrestrial sediment is bad for coral reef ecosystems. Coral Reefs 34:967–975
Stramski D, Reynolds RA, Kaczmarek S, Uitz J, Zheng G (2015) Correction of pathlength amplification in the filter-pad technique for measurements of particulate absorption coefficient in the visible spectral region. Appl Opt 54:6763–6782
Susanto RD, Zexun W, Adi TR, Zheng Q and others (2016) Oceanography surrounding Krakatau Volcano in the Sunda Strait, Indonesia. Oceanography 29:264–272
Tan KS, Acerbi E, Lauro FM (2016) Marine habitats and biodiversity of Singapore's coastal waters: a review. Reg Stud Mar Sci 8:340–352
Thrane JE, Hessen DO, Andersen T (2014) The absorption of light in lakes: negative impact of dissolved organic carbon on primary productivity. Ecosystems 17:1040–1052
Todd PA (2008) Morphological plasticity in scleractinian corals. Biol Rev Camb Philos Soc 83:315–337
Traina SJ, Novak J, Smeck NE (1990) An ultraviolet absorbance method of estimating the percent aromatic carbon content of humic acids. J Environ Qual 19:151–153
Urtizberea A, Dupont N, Rosland R, Aksnes DL (2013) Sensitivity of euphotic zone properties to CDOM variations in marine ecosystem models. Ecol Model 256:16–22
van Maren DS, Gerritsen H (2012) Residual flow and tidal asymmetry in the Singapore Strait, with implications for resuspension and residual transport of sediment. J Geophys Res Oceans 117:C04021
Vantrepotte V, Danhiez FP, Loisel H, Ouillon S, Mériaux X, Cauvin A, Dessailly D (2015) CDOM–DOC relationship in contrasted coastal waters: implication for DOC retrieval from ocean color remote sensing observation. Opt Express 23:33–54
Wauthy M, Rautio M, Christoffersen KS, Forsström L and others (2018) Increasing dominance of terrigenous organic matter in circumpolar freshwaters due to permafrost thaw. Limnol Oceanogr Lett 3:186–198
Weishaar JL, Aiken GR, Bergamaschi BA, Fram MS, Fujii R, Mopper K (2003) Evaluation of specific ultraviolet absorbance as an indicator of the chemical composition and reactivity of dissolved organic carbon. Environ Sci Technol 37:4702–4708
Welschmeyer NA (1994) Fluorometric analysis of chlorophyll *a* in the presence of chlorophyll *b* and pheopigments. Limnol Oceanogr 39:1985–1992
Weyhenmeyer GA, Fröberg M, Karltun E, Khalili M, Kothawala D, Temnerud J, Tranvik LJ (2012) Selective decay of terrestrial organic carbon during transport from land to sea. Glob Change Biol 18:349–355
Wijgerde T, van Melis A, Silva CIF, Leal MC, Vogels L, Mutter C, Osinga R (2014) Red light represses the photophysiology of the scleractinian coral *Stylophora pistillata.* PLOS ONE 9:e92781
Wit F, Rixen T, Baum A, Pranowo WS, Hutahaean AA (2018) The invisible carbon footprint as a hidden impact of peatland degradation inducing marine carbonate dissolution in Sumatra, Indonesia. Sci Rep 8:17403
Wong GTF, Ku TL, Mulholland M, Tseng CM, Wang DP (2007) The SouthEast Asian Time-series Study (SEATS) and the biogeochemistry of the South China Sea — an overview. Deep-Sea Res II 54:1434–1447
Yupi HM, Inoue T, Bathgate J, Putra R (2016) Concentrations, loads and yields of organic carbon from two tropical peat swamp forest streams in Riau Province, Sumatra, Indonesia. Mires Peat 18:14
Zepp RG, Shank GC, Stabenau E, Patterson KW and others (2008) Spatial and temporal variability of solar ultraviolet exposure of coral assemblages in the Florida Keys: importance of colored dissolved organic matter. Limnol Oceanogr 53:1909–1922
Zhou Y, Martin P, Müller M (2019) Composition and cycling of dissolved organic matter from tropical peatlands of coastal Sarawak, Borneo, revealed by fluorescence spectroscopy and parallel factor analysis. Biogeosciences 16: 2733–2749
Zhou Y, Evans CD, Chen Y, Chang KYW, Martin P (2021) Extensive remineralization of peatland-derived dissolved organic carbon and acidification in the Sunda Shelf Sea, Southeast Asia. J Geophys Res Oceans 126: e2021JC017292

Editorial responsibility: Toshi Nagata, Kashiwanoha, Japan
Reviewed by: H. Frigstad, A. Opdal and 1 anonymous referee

Submitted: December 18, 2020
Accepted: May 31, 2021
Proofs received from author(s): August 12, 2021